MICROWAVE PREPARATION AND APPLICATION OF ZnO-$ZnFe_2O_4$ COMPOSITE FOR PHOTOCATALYTIC DEGRADATION OF NAPHTHALENE IN OIL POLLUTION

BY

MAHMUD Aminu Dikko (B.ENG. ABU ZARIA, 2012)

P13EGCE8021

A DISSERTATION SUBMITTED TO THE SCHOOL OF POSTGRADUATE STUDIES, AHMADU BELLO UNIVERSITY, ZARIA

IN PARTIAL FULFILLMENT OF THE REQUIREMENTS FOR THE AWARD OF MASTERS OF SCIENCE DEGREE IN CHEMICAL ENGINEERING

DEPARTMENT OF CHEMICAL ENGINEERING

AHMADU BELLO UNIVERSITY, ZARIA

August, 2016

DECLARATION

I, MAHMUD Aminu Dikko do solemnly declare that this dissertation entitled 'Microwave Preparation and Application of ZnO-$ZnFe_2O_4$ Composite for Photocatalytic Degradation of Naphthalene in Oil Pollution' was carried out by me in the Department of Chemical Engineering, Ahmadu Bello University, Zaria. The information derived from the literature has been duly acknowledged in the text and the list of references provided. No part of this dissertation was previously presented for another degree or diploma at this or any other institution.

MAHMUD Aminu Dikko …… ……

Signature Date

CERTIFICATION

This dissertation entitled 'Microwave Preparation and Application of ZnO-$ZnFe_2O_4$ Composite for Photocatalytic Degradation of Naphthalene in Oil Pollution' by MAHMUD Aminu Dikko meets the regulations governing the award of Master of Science in Chemical Engineering of the Ahmadu Bello University, Zaria and is approved for its contribution to knowledge and literacy presentation.

Dr A. Hamza	…….……..	…….
Chairman, Supervisory Committee	Signature	Date
Dr B. Muktar	…….……..	…….
Member, Supervisory Committee	Signature	Date
Dr S.M. Waziri	…….……..	…….
Head of Department	Signature	Date
Professor Kabir Bala	…….……..	…….
Dean, School of Postgraduate Studies	Signature	Date

DEDICATION

This work is dedicated to my late wonderful father, Alhaji Zubair Mahmud, may *Aljannah Firdaus* be his final abode, amin. To my beloved mother, Hajiya Halima Mahmud, my two limits, Ai and Anna, my elder siblings, Amma, Babie, Billy and Zubby.

ACKNOWLEDGEMENT

I wonder if there is any one worth thanks like the God Almighty; for giving me the strength, the love, putting everyone in place for me at the very right time that I am in need, ranging from my parents who gave birth to me and guided me to school, my siblings that cared about me much, my teachers who taught me many of the things I know today, my lecturers who guided my academics tirelessly, my supervisors that created precious time out of their busy schedules, gave me listening ears, encouragement and guidance throughout this work, my friends who we walked up the hills down the mountains together, my loving foes that have kept my inspiration unaltered, my colleagues that we worked day and night in search for knowledge, my player haters who criticize all I do and in turn have to make all necessary amendments and finally, all those who have contributed to my success directly or indirectly, I have no words to say but may God bless you all.

ABSTRACT

Over the years, oil spillage has been precarious and most of the time unpredictable. It misbalances the ecosystem directly and indirectly on a rampage scheme, claiming thousands of marine lives; animals and plants and in some cases humans too. Whenever it occurs, the oil being less dense than water floats on it, which simply means that there is no limit to the extend it goes as most of the known part of the universe is connected by water. Conventional methods for tertiary oil spill containment are often energy intensive and require huge amount of sorbents and dispersants and in addition the methods do not destroy the pollutants in oil spills. In this work, ZnO-$ZnFe_2O_4$ composite was successfully synthesized using microwave combustion method. The molar ratio of Fe to Zn in the composite is 0.16. X-Ray Diffraction Analysis (XRD) shows that the synthesized ZnO-$ZnFe_2O_4$ composite is crystalline, and has very low crystallite sizes. The Scanning Electron Microscopy (SEM) image indicates that the ZnO-$ZnFe_2O_4$ composite is highly porous material with uniformly dispersed particles. Quadratic model was developed with R^2 value of 0.9993 and adjusted R^2 value of 0.9985, respectively. ZnO-$ZnFe_2O_4$ dosage and initial concentration of naphthalene have the largest effect on degradation process. The highest photocatalytic degradation of naphthalene was achieved at salinity of zero (that is in fresh water). The predicted optimum conditions for photocatalytic degradation of naphthalene using the ZnO-$ZnFe_2O_4$ composites are: initial naphthalene concentration of 16.8mg/L, ZnO-$ZnFe_2O_4$ dosage of 0.50 g/L, and salinity of 0 ppt. The experimental and the predicted values of naphthalene degradation under the predicted optimum values are 98.8 % and 99.04 % respectively. Hence, the developed quadratic model is reliable for predicting photocatalytic degradation of naphthalene.

TABLE OF CONTENTS

TITLE PAGE ..... **i**

DECLARATION ..... **iii**

CERTIFICATION ..... **iv**

DEDICATION ..... **v**

ACKNOWLEDGEMENT ..... **vi**

ABSTRACT ..... **vii**

TABLE OF CONTENTS ..... **viii**

LIST OF TABLES ..... **x**

LIST OF FIGURES ..... **xi**

ABBREVIATIONS ..... **xii**

CHAPTER ONE **1**
INTRODUCTION **1**

1.0 Preamble **1**

1.1 Problem Statement **3**

1.2 Research Justification **3**

1.3 Scope of the Work **4**

1.4 Aim and Objectives **4**

CHAPTER TWO **5**
LITERATURE REVIEW **5**

2.1 Introduction **5**

2.2 Oil spillage **5**

2.2.1 Causes of oil spill 6

2.2.2 Major oil spills around the world 7

2.2.3 Oil Spillage in Nigeria 9

2.2.4 Methods for removal of oil spill 10

2.3 Photocatalysis **13**

2.3.1 Types of photocatalysis 14

2.3.2 Uses of Photocatalysis 14

2.3.3 Factors affecting photocatalytic activity 15

2.3.4 Characterization of photocatalyst 17

2.4 Zinc Oxide (ZnO) 18

2.5 Zinc Ferrite ($ZnFe_2O_4$) 19

2.6 Mechanism of photocatalytic degradation of naphthalene 20

2.7 Measurement of concentration using UV-Vis spectroscopy 21

2.8 Previous related works 23

CHAPTER THREE 30
MATERIALS AND METHODS 30

3.1 Materials 30

3.2 Apparatus 30

3.3 Equipment 31

3.4 Methodology 32

3.4.1 Microwave preparation and characterization of the ZnO-$ZnFe_2O_4$ composite 32

3.4.2 Photocatalytic degradation of naphthalene using ZnO-$ZnFe_2O_4$ composite 33

CHAPTER FOUR 37
RESULTS AND DISCUSSION 37

4.1 Characterization of the synthesized ZnO-$ZnFe_2O_4$ composite 37

4.1.1 Chemical Composition of the ZnO-$ZnFe_2O_4$ composite 37

4.1.2 XRD Analysis of the ZnO-$ZnFe_2O_4$ composite 38

4.1.3 SEM Analysis of the Developed ZnO-$ZnFe_2O_4$ Photocatalyst..... 40

4.2 Photocatalytic degradation of naphthalene using the synthesized ZnO-$ZnFe_2O_4$ composite. 41

4.2.1 Modeling of photocatalytic degradation of naphthalene using the synthesized ZnO-$ZnFe_2O_4$ composite 42

4.2.2 Optimization of photocatalytic degradation of naphthalene using the synthesized ZnO-$ZnFe_2O_4$ composite 56

CHAPTER FIVE 59

CONCLUSIONS AND RECOMMENDATIONS 59

5.1 CONCLUSIONS 59

5.2 RECOMMENDATIONS 60

REFERENCES 61

LIST OF TABLES

Table 3.1: Design Summary including actual values of the uncoded factors for the photocatalytic degradation of naphthalene using the synthesized ZnO-$ZnFe_2O_4$ composite 32

Table 4.1: Chemical composition of the ZnO-$ZnFe_2O_4$ composite 37

Table 4.2: Design matrix for the photocatalytic degradation of naphthalene using the synthesized ZnO-$ZnFe_2O_4$ composite, experimental conditions and results of CCD model 43

Table 4.3: ANOVA for the developed model quadratic equation describing photocatalytic degradation of naphthalene using the ZnO-$ZnFe_2O_4$ composite 46

Table 4.4. Experimental and predicted values of naphthalene degradation under the predicted optimum values of the process variables 57

LIST OF FIGURES

Figure 2.1: Oil spill around the Niger Delta of the year 2015 (Shell Nigeria) ……10

Figure 3.1: Block diagram of the research methodology…….33

Figure 4.1: XRD pattern of the ZnO-$ZnFe_2O_4$ Composite ……...39

Figure 4.2: XRD pattern of $ZnFe_2O_4$ ……...39

Figure 4.3: XRD pattern of ZnO …….40

Figure 4.4: Response surface for simultaneous influence of initial concentration of naphthalene and ZnO-$ZnFe_2O_4$ dosage ……48

Figure 4.5: Response surface for simultaneous influence of initial concentration of naphthalene and salinity……49

Figure 4.6: Response surface for simultaneous influence of ZnO-$ZnFe_2O_4$ dosage and salinity……..50

Figure 4.7: Normal plot of residuals, normal percentile probability against residuals……51

Figure 4.8. Residual versus run plot……..……52

Figure 4.9: Plot of predicted values against actual values……. ……...53

Figure 4.10: Residual versus predicted plot …….54

Figure 4.11: Box-Cox plot for power transforms of photo degradation……55

ABBREVIATIONS

BET	Brunauer–Emmett–Teller
CNC	Colloidal Nanocrystal Clusters
DRS	Diffuse Reflectance Spectra
FT-IR	Fourier Transform Infra-Red Spectroscopy
HR-SEM	High Resolution Scanning Electron Microscopy
IR	Infra-Red Spectroscopy
MB	Methylene Blue
NP	Nanoparticles
PL	Photoluminescence
ppt	Parts Per Thousand
SEM	Scanning Electron Microscopy
TEM	Transmission Electron Microscopy
UV	Ultra-Violet
VSM	Vibrating Sample Magnetometer
XMCD	X-Ray Magnetic Circular Dichroism
XPS	X-Ray Photoelectron Spectroscopy
XRD	X-Ray Diffraction Analysis

CHAPTER ONE

INTRODUCTION

1.0 Preamble

Over the years, oil spillage has been precarious and most of the time unpredictable. It misbalances the ecosystem directly and indirectly on a rampage scheme, claiming thousands of marine lives; animals and plants and in some cases humans too. Whenever it occurs, the oil being less dense than water floats on it, which simply means there is no limit to the extend it goes as most of the universe is connected by water. Annually, an average of 5 million tons of petroleum is transported across the seas around the world (Hossain *et al.,* 2012). Thus, with this amount of transportation of oil to lacking areas which is inevitable, the oil spill occurrence becomes prevalent.

Numerous methods have been employed in addressing oil spillage problem, some of which include; burning of oil slick, mechanical techniques, biodegradation and the use of dispersants. Sorbents were also used, which include the synthetic organic, inorganic mineral and agricultural organic products, most of which are ineffective or expensive (Hossain *et al.,* 2012). Photocatalysis is applied in vast areas for the elimination of contaminants from water and air, odour control, bacterial inactivation, inactivation of cancer cells and a host of others (Casbeer *et al.,* 2012). Photocatalysis is a process in which the acceleration of a reaction occurs when a semiconductor interacts with light of sufficient energy to produce reactive oxidizing species which can lead to the photocatalytic transformation of pollutants, thus in the process yields hydroxyl radicals that can subsequently oxidize organic species producing mineral salts, carbon dioxide and water (Pelaez *et al.,* 2012). The mineral salt will be left in most cases in the water, the water

produced will increase the amount of water in the sea and the carbon dioxide may be used by sea plants for example planktons. Consequently, the removal of spilled oil on water can be achieved with the aid of photocatalysts (Magalhaes *et al.,* 2011).

TiO_2 and ZnO are the most widely investigated photocatalysts. However, they can only be used under UV irradiation. Present work focuses on ZnO-$ZnFe_2O_4$ composite that has a band gap capable of absorbing visible light and magnetic property that can be used during physical separation (Casbeer *et al.,* 2011). There are several methods for the preparation of composite of this nature which include; co-precipitation method, sol-gel method, ultra-sound auto combustion method, ordinary combustion method, microwave combustion method and a host of others. In this work, the microwave combustion method was adopted to increase efficiency of ZnO-$ZnFe_2O_4$ composite by reducing particle size growth (Feng *et al*., 2015).

Naphthalene is often used as a model of polycyclic aromatic hydrocarbons that are present in petroleum and petroleum products. Naphthalene can be frequently found in oil produced water and oil spills. Naphthalene is the most water-soluble polycyclic aromatic hydrocarbon. Naphthalene belongs to the class of persistent organic pollutants of special concern because it has both acute and chronic effects on human beings and animals (Irwin *et al.*, 1997). This dissertation focuses on microwave assisted preparation of ZnO-$ZnFe_2O_4$ composite and its application for photocatalytic degradation of naphthalene under visible light irradiation. The work also covers modeling and optimization of photocatalytic degradation of naphthalene using the synthesized ZnO-$ZnFe_2O_4$ composite using the response surface methodology.

1.1 Problem Statement

i. Annually, an average of 5 million tons of petroleum is transported across the seas around the world (Hossain *et al.,* 2012). Petroleum mixtures contain approximately 0.25 % naphthalene (Potter and Simmons, 1998) thus; 12 500 tons of naphthalene annually on the average stands a risk of spillage which may lead to loss of aquatic lives and contamination of water, sea shores, harbours, beach side etc.

ii. Conventional methods for tertiary oil spill containment are often energy intensive and require huge amount of sorbents and dispersants and in addition the methods do not destroy the pollutants in oil spills.

iii. Difficulty in the removal of trace amounts of toxic polarizable aromatic pollutants in water.

iv. Despite its popularity, ZnO-$ZnFe_2O_4$ composite as a visible light active photocatalyst, it has never been used for photocatalytic degradation of naphthalene.

v. The effect of salinity on photocatalytic degradation of naphthalene is lacking in the literature.

1.2 Research Justification

i. Photocatalysis is an environmentally friendly process that can be driven by solar energy.

ii. Photocatalysts can be used continuously, i.e. in many cycles with little or no labour.

iii. ZnO-$ZnFe_2O_4$ composite can be readily produced in large quantities using microwaves. iv. ZnO-$ZnFe_2O_4$ composite can easily be separated from water using magnets.

v. Protecting human being and aquatic lives from the hazardous effects of oil spillage.

vi. Availability of data on the effects of process parameters on photocatalytic degradation of naphthalene.

1.3 Scope of the Work

The scope of this work is limited to preparation and application of $ZnO\text{-}ZnFe_2O_4$ composite for photocatalytic degradation of naphthalene in fresh water and model sea water.

1.4 Aim and Objectives

The aim of this work is to prepare $ZnO\text{-}ZnFe_2O_4$ composite via microwave combustion method, characterize and apply the composite for photocatalytic degradation of naphthalene (a model of aromatic compounds present in petroleum and its products) in fresh water and model sea water.

The specific objectives are to:

i. prepare $ZnO\text{-}ZnFe_2O_4$ composite using microwave combustion method.

ii. study the phase composition of the composite by XRD, and surface morphology by the use of SEM analyses.

iii. study the effects of photocatalyst ($ZnO\text{-}ZnFe_2O_4$ composite) dosage, initial concentration of naphthalene and salinity on its degradation.

iv. determine the optimum conditions for the photocatalytic degradation of naphthalene under visible light illumination.

CHAPTER TWO

LITERATURE REVIEW

2.1 Introduction

This chapter discusses oil spillage in general and oil spillage in Nigerian coast; causes of oil spill, major oil spills ever recorded with their effects and intensity, factors affecting oil spillage, repression and removal of oil spill, photocatalysis, types of photocatalysis, uses of photocatalysis, factors affecting photocatalytic activity, methods of enhancing the activity of the photocatalysts, characterization of photocatalysts, ferrites synthesis methods, $ZnO\text{-}ZnFe_2O_4$ as a photocatalyst and previous works done in resolving the problem.

2.2 Oil spillage

An oil spill is oil discharged accidentally or intentionally that floats on the surface of water bodies as a discrete mass and is carried by wind, currents and tides. In addition, oil spills can be partially controlled by chemical dispersion, combustion, mechanical containment and adsorption.

Furthermore, they have destructive effects on coastal ecosystems.

The main factors affecting oil spillage control over the years include (Hossain *et al.*, 2012):

i. Sea conditions; this is the most critical factor affecting spill control and it is described in terms of wave height and period. Wave heights of 1-2 ft and periods of 1-3S render most booms ineffective. Also, wave heights above 6 ft make control operations difficult for small vessels.

ii. Wind velocity and direction; these are the most vital factors controlling slick movement over open water. In oceans, wind spreads oil more than currents or waves, with a velocity between 3 and 10% of that of the wind. Hence, within minutes of a spill, oil spreads to

cover hundreds of square yards and within an hour, it covers hundreds of square miles. This makes early confinement necessary to limit the spread of an oil spill; reduce the area of contamination; prevent oil from entering drains, sewers, or water courses; and of course, make cleanup operations easier. Thus, local wind data are useful in predicting slick movement and in planning spill control actions.

iii. Currents and tides; sea current velocity of one knot or more tends to build up hydraulic forces against floating booms, causing oil to flow and escape under the boom. Similarly, large tidal ranges complicate shoreline protection and cleanup.

iv. Temperature and atmospheric conditions; high temperature causes more evaporation of lighter fractions of oil and increases the tendency of heavier fractions to persist on water surfaces, which in turn can reduce the effectiveness of chemical dispersant on the highly viscous and thicker crude and also make the oil unable to sustain combustion. Also, rain, snow, or fog may make accessibility to the spill area difficult.

2.2.1 Causes of oil spill

Even though oil spill may occur as a result of different factors, the common causes are as follows:

i. Equipment faults in oil tankers; this occurs when oil tankers break down which perhaps get stuck on the shallow land where abrasion may cause a hole in the tanker that may lead to large amount of oil being released into the oceanic bodies. Though, only 2% of oil in water bodies is as a result of this action.

ii. From nature and human activities on land; the large majority of oil spilled is from natural seeps, geographical seeps from the ocean floor as well as leaks that occur when products using petroleum or other forms of oil are used on land and oil is washed off into water bodies.

iii. Water sports; this include spills by petroleum users of released oil, it happens when various water sports or water vehicles such as motor boats and jet skis leak fuel.

iv. Drilling work carried out in the sea; this occurs as a result of drilling work carried out in the sea, the oil and petroleum used for such activities are released into the sea, therefore, causing an oil spill.

v. There are many more causes, which can be related to accidents and lack of proper equipment maintenance.

2.2.2 Major oil spills around the world

Some of the major oil spillages recorded in history, the incidence, the amount of oil spilled, the length of affected areas, some of the cost implications, the environmental effect and the clean up technique used include:

i. Torrey Canyon**;** this occurred in 1967, off the English Channel in the Atlantic Ocean about 120 000 tons of crude oil was spilled, 161 km of coast line was affected, an estimate of 25 000 birds died. The clean up techniques used include; natural weathering, the use of dispersants, bombs for the in-situ ignition, straws and gorse were also used on the sandy beaches.

ii. Liberian Registered Tanker; this occurred in 1970 at Chedabucto Bay, Nova Scotia about 16 000 tons of oil spilled, 306 km of coast line was affected. The clean up techniques used include; floating booms were used though were less successful and skimmers and sorbents were successful.

iii. Amoco Cadiz; this occurred in 1978, off the Coast of Brittany, France, about 230 000 tons of light crude was spilled, 300 km of coast line was affected, an estimate of over 3 450 sea birds died not to talk about the fisheries, oysters and sea weeds that were immensely affected and the cost implication was $ 282 million (₦47.235 billion) lost where as $ 85 million (₦14.2375 billion) was paid as fine. The clean up techniques used include; microbial degradation, mechanical removal of oil on shore, pressure washing with water, rubber powder and sinking agents were employed though was less successful.

iv. Exxon Valdex; this occurred in 1989 in Prince Williams sound Alaska about 30, 531.56 tons of crude was spilled, 1 900 km of coast line was affected, an estimate of 250, 000 birds, 2,800 sea otters, 250 bald eagles, 22 killer whales died and the cost implication was $ 2.1 billion (₦ 351.75 billion) used for clean up and $ 7 billion (₦ 1.1725 trillion) was paid as fine. The clean up techniques used include; booms, dispersants though less successful, in situ burning, sorbents were used, warm water flushing of the beach and also bioremediation aided the clean up process.

v. Gulf War; this occurred in 1990 in Kuwait about 1, 000, 000 tons of crude was spilled, an estimate of 20, 000 birds died. Here, the wells were set ablaze.

vi. Sea Empress; this occurred in 1996, over 70, 000 tons of crude was spilled, 100 km of coast line was affected, an estimate of 2, 200 birds died, sea weeds and shell fishes were affected and the cost implication was $ 60 million (₦ 10.05 billion) lost where as $ 37 million (₦ 6.1975 billion) was used for clean up. The clean up techniques used include mechanical removal and some were removed with chemical dispersants.

vii. BP Gulf of Mexico; this occurred in 2010, about 576, 470 tons of crude was spilled, 790km of coast line was affected, an estimate of 997 birds died, 400 sea turtles, 47 mammals including Dolphins and the cost implication for the lost of marine lives was $ 5.4 billion (₦ 904.5 billion) lost where as $ 21 billion (₦ 3.5175 trillion) was paid for gross negligence and $ 20 billion (₦ 3.350 trillion) was paid as compensation and for clean up. The clean up techniques used include; booms and skimmers, dispersants and controlled burning (Hossain *et al.,* 2012) . The exchange equivalent rate was taken as at 02/12/2014 at ₦167.5 to $1.

2.2.3 Oil Spillage in Nigeria

Nigeria has a coastline of approximately 853km facing the Atlantic Ocean. This coastline lies between latitude 4^0 10^1 to 6^0 20^1 N and longitude 2^0 45^1 to 8^0 35^1 E. The Nigerian coast is composed of four distinct geomorphology units namely the Barrier-Lagoon Complex; the Mud Coast; the Arcuate Niger Delta and the Strand Coast. In 1956, Royal Dutch Shell discovered crude oil at Oloibiri, a village in the Niger Delta, and commercial production began in 1958. Today, there are about 606 oil fields in the Niger Delta, of which 360 are on-shore and 246 offshore. Nigeria was the largest oil producer in Africa and the sixth largest in the world, averaging 2.7 million barrels per day (bbl/d) in 2006. Nigeria's proven oil reserved is 35.2 billion barrels. Nigeria's economy is heavily dependent on earnings from the oil sector, which provides 20% of GDP, 95% of foreign exchange earnings, and about 65% of budgetary revenues. Since the discovery of oil in Nigeria in 1956, the country has been suffering the negative environmental consequences of oil exploration and exploitation. Between 1976 and 1996 a total of 4 647 incidents resulted in the spill of approximately 2,369,470 barrels of oil into the environment. In addition, between 1997 and 2001, Nigeria also recorded a total number of 2,097 oil spill incidents. In 1998, forty thousand barrels of oil from Mobil platform off the Akwa Ibom coast

were spilt into the environment causing severe damage to the coastal environment. Several oil spill management policy and efforts are in place to reduce the menace of oil spill incidents in the country. Some of these policies and efforts were made by the Federal Government, Non governmental agencies and oil firms in the country. Thus, there is an immense need to develop indigenous control measures of oil spill.

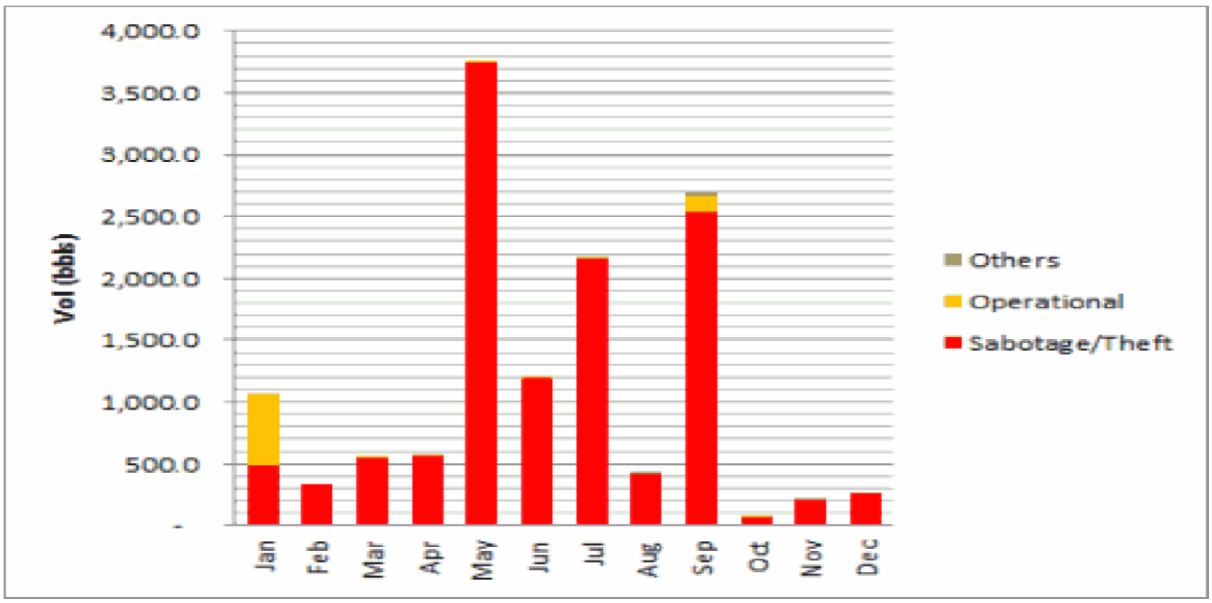


Figure 2.1: Oil spill around the Niger Delta of the year 2015 (Shell Nigeria)

2.2.4 Methods for removal of oil spill

There are various cleanup methods and there is no simple procedure which can be recommended for all spills. Spilled oil will behave differently depending on the type of oil, the surface on which it spills the soil, subsoil conditions, the prevailing weather conditions and many more. Therefore, the choice of cleaning method must take into account these conditions. In most cases, two or more methods are combined to achieve an effective cleanup. Some of the various cleanup methods include:

i. In-situ burning; this technique involves burning a thick oil slick on the water surface. It helps by reducing the amount of oil on the water's surface and therefore reduces the hazards of the

oil slick on the ecosystem and the environment. It can remove 600-1800 barrels (100300 tons) of oil per hour. Ignition of an oil spill is done using a device such as a helitorch suspended beneath a helicopter. The advantage of in-situ combustion is, in ice or cold water application where mechanical booms and chemical dispersants have limited efficiency whereas all conditions favoring combustion tend to persist for a long time since ice strongly influences weathering. Though in-situ burning is effective if the following conditions are in place; the oil slick is sufficiently wide so that a good volume of oil is burnt off at a time, the oil is very thick to sustain combustion, the water is calm and the slick location is distant from sensitive facilities. However, because of sea weather conditions all of these conditions hardly exist for a long time and for this reason in-situ burning is limited. Other limitations of in-situ burning include; Ignition of the oil, maintaining combustion of the slick, generation of large quantities of smoke, viscous residue and safety concerns (Hossain *et al.,* 2012).

ii. Mechanical techniques; this involves the use of booms spread over surface of seas, estuaries and coastal waters to prevent the spread of oil slicks or to direct their movements.

Booms are combined to make "V" shaped barriers, which concentrate the oil for pickup by skimmer barges and boats. The advantage of booms and skimmers over other commonly used methods such as chemical dispersants and in-situ combustion is the absence of adverse environmental effects. This technique is expensive, and requires large number of personnel and equipment (Hossain *et al.*, 2012).

iii. Bioremediation; this is a process by which small organisms like bacteria, yeasts, and fungi break up complex compounds into smaller compounds for their food. This process occurs naturally. Its application in oil spill cleanup involves the artificial introduction of biological agents such as fertilizers and nutrients to native microorganisms in the contaminated site.

Bioremediation is ineffective in removing oil spills that consist of large coherent masses or for sunken oil spills also limited by abiotic environmental factors such as low level of nutrients including phosphate and fixed forms of nitrogen, very low temperatures, and insufficient oxygen (Hossain *et al.,* 2012).

iv. Dispersion; Surfactants (dispersants) are partially soluble in both oil and water. When sprayed on an oil slick, surfactants reduce the interfacial tension between the oil and water. This enhances dispersion and increases the natural dilution and biodegradation process of oil in water. Dispersants are expensive and may contain toxic compounds harmful to aquatic fauna and flora and also ineffective in calm waters i.e. more effective in tumultuous waters were mixing of the dispersants and the oil is expected (Hossain *et al.,* 2012).

v. Sorption; this involves the use of materials that are oleophilic and hydrophobic, i.e., they have a high capacity to sorb oil and repel water. There are three classes of sorbents synthetic organic, inorganic mineral and agricultural (organic) products. The efficiency of a sorbent depends on its recyclability, wettability, density, geometry, sorption capacity and sorption rate. These properties determine the time required to spread and harvest the sorbents. Sorbents have been recorded to be one of the most effective and cheapest methods of cleaning oil spills on shorelines. Mineral sorbents are generally disliked as they have numerous shortcomings, such as contamination of sea beds and harmful effects to aquatic habitats, the non biodegradability of synthetic sorbents is a major disadvantage and the limitations of agricultural sorbents include high cost (Hossain *et al.*, 2012).

All the cleanup methods discussed have various limitations that make it necessary to synthesize a composite that will be efficient, cheap, effective, harmless to both fauna and flora and to the ecosystem and also easily be removed and reused.

2.3 Photocatalysis

In simple term, photocatalysis is the speeding up of photoreaction in the company of a catalyst (John, 2014). It is used to describe a process in which the acceleration of a reaction occurs when a semiconductor material comes in contact with light of sufficient energy or in other words, light of certain wavelength to produce reactive oxidizing species that are capable of orchestrating photocatalytic transformation of substances mostly of organic origin. In the photocatalytic reaction, two main things occur first, the oxidation of dissociatively adsorbed water by photogenerated holes and second, the reduction of an electron acceptor by photoexcited electrons. Photocatalysis can thereby be said to mean, photon-assisted generation of catalytically active species. If the initial photoexcitation process occurs in an adsorbate molecule which then interacts with the ground state of the catalyst substrate, the process is referred to as catalysed photoreaction. But when the initial photoexcitation takes place in the catalyst substrate and the photoexcited catalyst then interacts with the ground state adsorbate molecule, the process is referred to as sensitized photoreaction. Heterogeneous photocatalysis refers to semi conductor photocatalysis or semiconductor sensitized photoreaction. In photocatalysis, light of energy greater than the band gap of the semiconductor excites an electron from the valence band to the conduction band, thereby generating a positive hole in the valence band. Charged carriers can then migrate to the catalyst surface and initiate redox reaction with adsorbates, the positive holes can then oxidize water at the surface to produce OH-radicals that are extremely strong oxidants. The hydroxyl radicals can therefore, oxidize the organic species with mineralization producing mineral salts, carbondioxide and water (Pelaez *et al.*, 2012).

2.3.1 Types of photocatalysis

There are basically two types of photocatalysis; homogenous and heterogeneous photocatalysis. In homogenous photocatalysis, the reactants and photocatalyst exist in the same phase; examples

include the transition metal oxide, ozone and photo-Fenton systems. On the other hand, heterogeneous photocatalysis occurs when the reactants and photocatalyst exist in different phases, this wing of photocatalysis involves a large variety of reactions which include, water detoxification, gaseous pollutant removal, hydrogen transfer, dehydrogenation, mild and total oxidations, to mention but a few.

In general, recombination is a huge downfall or limitation for a semiconductor photocatalyst. It occurs when the excited electron by the absorption of light energy, falls back to the valence band without reacting with the adsorbed species to foster the photocatalytic reaction thereby rendering the goal of the photocatalysis insurmountable (Palaez *et al.*, 2012).

2.3.2 Uses of photocatalysis

The uses of photocatalysis in this modern day cannot be over emphasized with the advent of nanotechnology. Some of the applications include:

i. hydrogen generation
ii. water purification
iii. self sterilization and self cleaning coatings
iv. air pollution control
v. photocatalytic lithography
vi. photocatalytic metal corrosion prevention
vii. petrochemical production

Though, the hydrogen generation is focused on the future energy demands, the water purification, air pollution as well as self sterilization can be carried out by cashing in on the wide band gap of

transition metal oxides like ZnO and TiO_2 for its ability to remain super-hydrophilic and retain the property after light ceased for a while (John, 2014).

2.3.3 Factors affecting photocatalytic activity

Some of the factors bound to affect the activity of a photocatalyst include;

i. Band structure - the general understanding of the mechanism of photocatalysis is based on photoabsorption of a semiconducting material which excites electrons from the valence band to the conduction band leaving positive holes in the valence band and an electron hole pair is generated (Palaez *et al.,* 2012) ii. Band gap - to comprehend the band gap, there is the need to understand the band theory. The band theory states that delocalized electrons move freely through bands formed by overlapping molecular orbitals. There exist two bands, the valence band and the conduction band. In metals, immediately after the valence band is the conduction band. In semiconductors and insulators, in between the valence band and the conduction band there exist the energy gap. This energy gap accounts for the photocatalysis. In the semiconductors, the energy gap is very small, that is in between 0 and 5eV. In conductors it is 0eV, therefore there is no energy gap from valence band to conduction band. Whereas insulators energy gap is greater than 5eV which makes it absolutely impossible for electric conduction or photocatalysis to take place. Taking advantage of the energy gap in semiconductors, energy gap is being reduced by doping or coupling with other semiconductors to improve photocatalysis (Chang, 2005).

iii. Crystallinity - photocatalyst are often inorganic solid materials that are usually crystals and the crystalline form is determined by an X-ray Diffraction pattern. Crystalline particles are detected by XRD peaks where amorphous materials exhibit no diffraction peaks. The more

sharp the XRD pattern, the more crystalline the material being investigated and this is being used to determine how crystallites grow to be larger sized particles (John, 2014).

iv. pH of the medium - the pH of any medium is the concentration of hydrogen ions in solution and it indicates the level of acidity or alkalinity of an aqueous solution (Abdulhamid et al., 2013). pH is the negative logarithm of the hydrogen ion concentration. The acidity of an aqueous solution is expressed as its pH; at 25^0C an acidic solution has pH less than 7 and a basic solution has pH greater than 7. A neutral solution has pH of 7 (Chang, 2005).

v. Specific surface area - the photocatalytic activity of a semiconductor photocatalyst involves adsorption of the compound to be oxidized and trapping of holes and electrons on the catalyst surface. The surface area of a photocatalysts determines the number of adsorption sites. The smaller the particle size the greater the surface area and the better the adsorption (John, 2014).

vi. Photocatalyst dosage - there are numerous studies on the influence of catalyst concentration on process efficiency. It can be deduced that incident radiation on the reactor and length of path inside the reactor are fundamental in determining optimum concentrations. Thus, if the radiation comes from a source placed outside the photoreactor as in a reactor illuminated by solar radiation (John, 2014). The photocatalyst dosage helps in ascertaining the optimum amount of photocatalyst that can be used and can be obtained through varying the amount.

vii. Pollutant type and concentration - each pollutant may behave differently in photocatalysis. Some pollutants may aid or impede photocatalysis.

viii. Salinity - Salinity is a measure of dissolved salt mostly NaCl in water. It is usually highest during periods of low flows and increases as water levels increases. Salinity is measured as either Total Dissolved Solids (TDS) which measures the amount of salt dissolved in water or as Electrical conductivity (EC) which is a property that enables the conduction of electricity (Abdulhamid et al., 2013).

2.3.4 Characterization of photocatalyst

Solid photocatalyst characterization is usually being conducted with the aid of analytical techniques which include:

2.3.4.1 X-ray Diffraction - x-rays can be used to obtain objects on the atomic and molecular scale whose wavelengths range about 0.01 nm to 10 nm. Though X-rays cannot be focused, so they do not produce well formed images. X-ray diffraction refers to the scattering of Xrays by the units of a crystalline solid. The scattering or diffraction patterns produced are used to deduce the arrangement of particles in a solid lattice. In 1912, the German physicist Max von Laue correctly suggested that, because the wavelength of X-rays is comparable in magnitude to the distances between lattice points in a crystal, the lattice should be able to diffract X-rays. An X-ray diffraction pattern is the result of the interference of the waves associated with X-rays (Chang, 2005). X-ray diffraction provides detailed information on the crystallographic structure and physical properties or materials and thin films. It is used to examine the crystal structures of photocatalyst particles (John, 2014).

2.3.4.2 X-ray Florescence spectroscopy; this is the emission of characteristic secondary (or fluorescent) x-rays from a material that has been excited by bombarding with high energy X-

rays or gamma rays. It is widely used for elemental and chemical analysis of minerals (John, 2014).

2.3.4.3 Scanning electron microscopy; the electron microscope is an extremely valuable application of the wavelike properties of electrons because it produces images of objects that cannot be seen with the naked eyes or with light microscopes. By the laws of optics, it is impossible to form an image of an object that is smaller than half the wavelength of the light used for the observation. Thus, since the range of visible light wavelengths starts at about 4×10^{-5}cm, anything smaller than 2×10^{-5}cm cannot be seen. Electrons, are charged particles which can be focused in the same way the image in a TV screen is focused by simply applying an electric field or a magnetic field. Thus, since the wavelength of an electron is inversely proportional to its velocity, by accelerating electrons to very high velocities, shorter wavelengths as 0.004nm can be obtained (Chang, 2005).

2.3.4.4 UV-Vis Diffuse Reflectance spectroscopy; this provides an indication of the visible light activity of a photocatalyst. Diffuse reflectance spectra are obtained with UV-vis spectrometer and can be converted from refelection to absorption spectra by the KubelkaMunk method (John, 2014).

2.4 Zinc Oxide (ZnO)

Zinc oxide, ZnO is an inorganic compound that is insoluble in water. It occurs naturally as zincite, though mostly is being synthesized as white powder and used as an additive in plethora materials and products including rubber, plastic, ceramic, glass and a host of others. Other names include; flowers of zinc, Chinese white, philosopher's wool, calamine or zinc white. It has a molar mass of

81.38g/mol, it is odorless white solid with a density of 5.606g/cm^3. It has a melting point and boiling point of 1975^{0}C. It is insoluble in water and has a band gap of 3.3eV. This semiconductor has several properties including good transparency, high electron mobility, wide band gap and strong room temperature luminescence.

2.5 Zinc Ferrite ($ZnFe_2O_4$)

Zinc ferrites are series of synthetic inorganic compounds of zinc and iron, with a general formular $Zn_xFe_{3-x}O_4$. Various methods are employed in ferrites synthesis, such methods include (Casbeer *et al.*, 2012):

i. Sol-gel and citrate method ii. Co-precipitation method iii. Solid state reaction method and iv. Thermal methods which include;

- Hydrothermal method
- Solvothermal method
- Mechanothermal method and
- Microwave combustion method

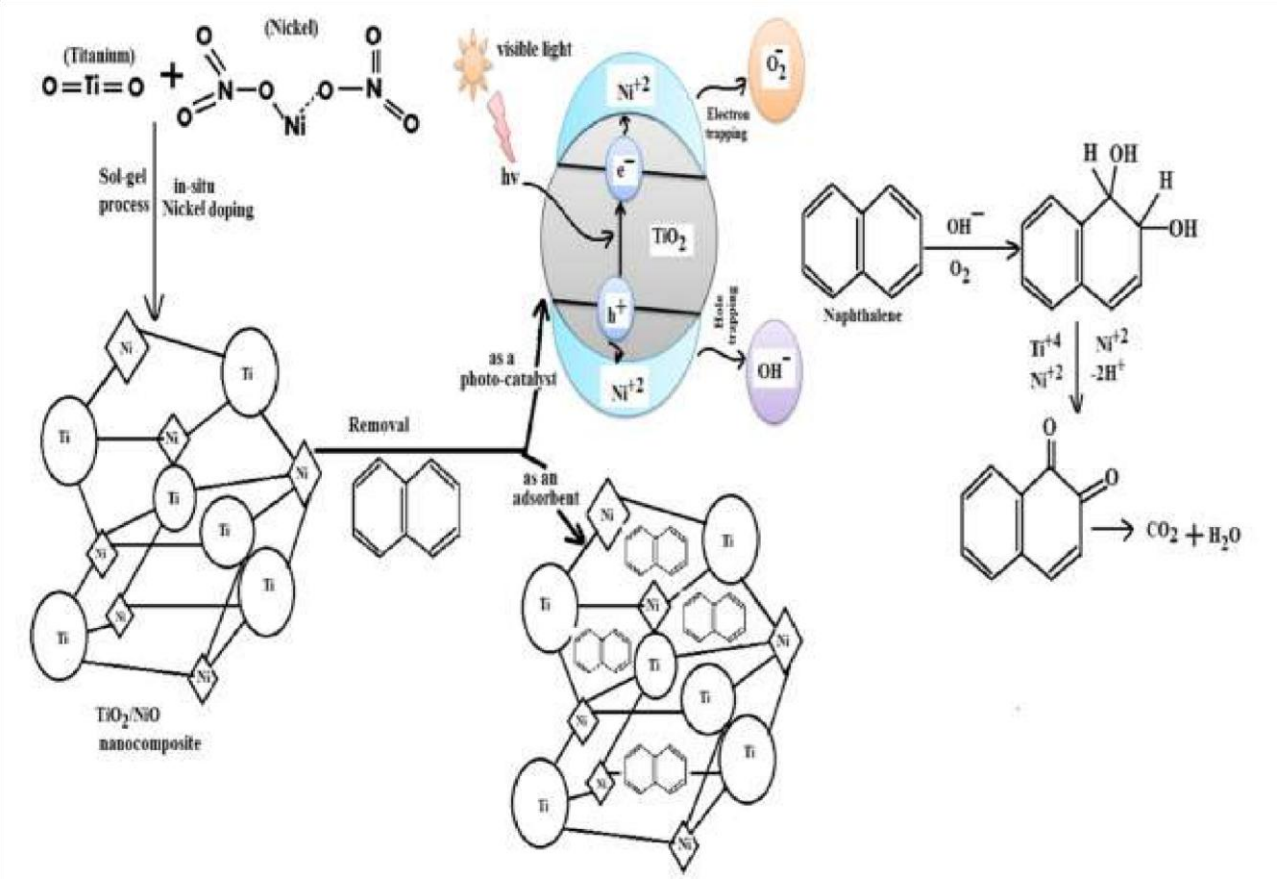
In general, all the above methods require a high temperature and a very long period of time for the ferrites to be formed with the exception of microwave combustion method which uses a short period of time (few minutes) and thus, giving no time for grain growth thereby allowing fine particles with high specific surface area to be obtained (Feng *et al.*, 2015). They can be prepared by aging solutions of $Zn(NO_3)_2$, $Fe(NO_3)_3$ and triethanolamine in the presence and in the absence of hydrazine or by reacting iron oxide and zinc oxide at high temperature. The spinel

$(Zn,Fe)Fe_2O_4$, is a tan-colored solid, insoluble in water, acids or diluted alkali, they are used as pigments especially in areas requiring heat stability. Zinc ferrite is paramagnetic in bulk but ferromagnetic in nanocrystalline thin film format. Though, it can also occur in natural form as Franklinite, $ZnFe_2O_4$ named after Franklin Mine that discovered it in the 1819. It usually contains 5-10wt% ZnO and 10-15wt% Fe_2O_3. The nanoparticles have a purity of 98.5%, APS of 10-30nm, bulk density of ~0.5g/$cm^3$and true density of ~5.1g/cm^3, saturated magnetization of 4.0emu/g and remanent magnetization of 0.06 emu/g. It is brown in color and the morphology is spherical.

2.6 Mechanism of photocatalytic degradation of naphthalene

Recently, Lee and Sharma (2015) proposed a mechanism of photocatalytic degradation of naphthalene using NiO-TiO_2 composite (Scheme 1). The process begins in the dark phase, and begins with the adsorption of the nonpolar organic moieties onto the hydrophobic surface of a photocatalyst and gets combined with monolayer surface until saturation. Then, adsorption through heterogeneity occurs by means of interaction of the previously adsorbed organic moieties with the organic compound to be adsorbed. This naphthalene is adsorbed onto the surface of a photocatalyst through hydrophobic bonding force. However, in light phase, the photocatalyst also plays an important role for the naphthalene removal. In the photocatalytic process, photo-excitation occurs by the incident photon energy which requires higher than the band gap energy. The photocatalyst generates electron hole pairs during irradiation of visible light. The electrons trapped by nickel are scavenged not by superoxide radicals but by oxygen molecules. The electron transfer to oxygen molecules produces radicals of superoxide. Moreover, surface of the photocatalyst is hydrated due to the reaction with -OH ions or with H_2O by the transfer of electron through localized holes to form more hydroxyl radicals. These hydroxyl radicals and superoxide are strong oxidants and can enhance the degradation of naphthalene. Thus, a large

amount of hydroxyl radicals can lead to mineralization and transformation of naphthalene into CO_2 and H_2O (Lee and Sharma, 2015).



Scheme 1: Proposed mechanism for photocatalytic degradation of naphthalene using TiO_2/NiO nanocomposite (Lee and Sharma, 2015).

2.7 Measurement of concentration using UV-Vis spectroscopy

Ultraviolet-Visible (UV-VIS) spectroscopy is often used to measure the concentration of compounds that have chromophores attached to them in solutions using Beer Lamberts law. Molecules absorb energy and this energy can bring about translational, rotational or vibrational motion or ionization of the molecules depending upon the frequency of the electromagnetic

radiation they receive. Excited molecules are unstable and quickly drop down to ground state again giving off the energy they have received as electromagnetic radiation. The wavelength and intensity of the electromagnetic radiation absorbed or emitted can be recorded to get a spectrum. Spectral analysis yields qualitative and quantitative information about the matter under study. UV-Vis spectroscopy is useful to characterize the absorption, transmission, and reflectivity of a variety of compounds and technologically important materials, such as pigments, coatings etc. The UV-VIS spectra have broad features that are used for sample identification but are very useful for quantitative measurements. UV-VIS spectroscopy studies the electronic transitions of molecules as they absorb light in the UV and visible regions of the electromagnetic spectrum. The data is used to produce absorbance spectra.

The visible region of the spectrum comprises photon energies of 36 to 72 Kcal/mole, and the near ultraviolet region, up to 200 nm, extends this energy range to 143 kcal/mole. This energy is enough to promote the outer electrons to higher energy levels. As a rule, the energetically favored electron promotion will be from the Highest Occupied Molecular Orbital (HOMO) to the Lowest Unoccupied Molecular Orbital (LUMO). The resulting species is said to be in an excited state. An optical spectrometer records the wavelengths at which absorption occurs, together with the degree of absorption at each wavelength to produce a spectrum.

UV absorptions of molecules are generally broad because vibrational and rotational levels are "superimposed" on top of the electronic levels. In addition to undergoing electronic transitions the atoms can rotate and vibrate with respect to each other. These vibrations and rotations also have discrete energy levels. This large number of available levels produces multiple absorptions and appearance of broad bands in Uv/Vis spectrum, rather than narrow peaks. For this reason, the wavelength of maximum absorption (λ_{max}) is usually reported.

Beer – Lambert Law is central to spectrophotometry and for many current applications a spectrometer is increasingly becoming the measurement device of choice. This law forms the basis of nearly all the chemometric methods for spectroscopic data. Simply stated, the law claims that when a sample is placed in the beam of a spectrometer, there is a direct and linear relationship between the amount (concentration) of its constituent(s) and the amount of energy it absorbs.

In mathematical terms:

$$\text{Absorption (A)} = -\log\left(\frac{\text{P}}{\text{Po}}\right) = \varepsilon\text{bc} \ldots\ldots\ldots\ldots\ldots\ldots\ldots\ldots\ldots\ldots\ldots\ldots\ldots\ldots\ldots\ldots\ldots\ldots\ldots\ldots.2.1$$

where A is the sample's Absorbance value at specific wavelength (or frequency), P is the intensity o of incident light, P is the intensity of transmitted light , ε is the absorptivity coefficient of the material (constituent) at that wavelength, b is the path length through the sample and c is the concentration. The absorptivity coefficient for every material is different, but for a given compound at a selected wavelength, this value is a constant; ε is also known as molar extinction coefficient.

2.8 Previous related works

Srinivasan *et al.,* (2006) reported a new co-precipitation/hydrolysis method for the synthesis $TiO_2ZnFe_2O_4$ nanocomposite that is directed towards extending the photoresponse of TiO_2 from UV to visible wavelengths (> 400 nm). The effect of TiO_2's accelerated anatase-rutile phase transformation due to the presence of the coupled $ZnFe_2O_4$ narrow-bandgap semiconductor is evaluated and it was concluded that the narrow-band gap semiconductor $ZnFe_2O_4$ can be effectively coupled with TiO_2 for visible-light (> 400 nm)-activated photocatalysis. The

transformation's dependence on pH, calcinations temperature, particle size, and $ZnFe_2O_4$ concentration has been analyzed using XRD, SEM, and UV-visible spectrometry. The study shows the potential of inexpensive and nontoxic photocatalysts for indoor visible-light applications (Srinivasan *et al.*, 2006).

$ZnFe_2O_4$, with high crystallinity, high surface area, and homogeneity has been successfully synthesized by Borse *et al.* (2006) using the polymer complex method. A pure phase $ZnFe_2O_4$ was obtained at a relatively lower temperature of 900^0C. The as-synthesized nanoparticles are agglomerates of crystals with an average size of ~50 nm, as estimated from the X-ray diffraction analysis. The band gap of the n-type semiconducting metal oxide, as determined using an ultraviolet-visible diffuse reflectance spectrometer was found to be 1.90eV (653 nm). The photocatalytic activity of $ZnFe_2O_4$ was investigated by using the photoreduction of water under visible light (~420 nm), which was found to be much higher than that of the well-known TiO_2−xNx photocatalyst. This superior performance was attributed to the larger surface area, the uniform and well-dispersed deposition of the Pt co-catalyst over the surface, and the small band gap of the chemically-prepared ferrite photocatalyst (Borse *et al.*, 2009).

Moradi *et al*(2012) prepared TiO_2/ZnO nanocomposite with different molar ratios of ZnO: TiO_2 using the sol-gel method. XRD study showed that the crystallization behavior of the nanocomposites was dependent with the molar ratios of ZnO. The SEM images indicated that with increasing the molar ratios of TiO_2/ZnO until 50:10, regular morphology can observed and is of interest for catalytic purposes since it expectantly improves the surface area. The photocatalytic activity of the synthesized nanocomposite was investigated for decolourization of methylene blue in water under UV irradiation in a batch reactor. The results indicated that the photocatalytic activity of the nanocomposite with 50:10 M ratio of TiO_2/ZnO was the best and

also addition of high dose of ZnO to TiO_2 decreases the light penetration and also reduces the degradation rate (Moradi *et al.,* 2012).

Sun *et al*. (2012) synthesized $ZnFe_2O_4$ with spinel structure by an improved solution combustion method through a facile and environmentally friendly path way and their photocatalytic activity under visible light radiation was investigated. The particle synthesized under the ignition temperature of 573 K has a pure phase. While a small amount impurities, α-Fe_2O_3 and ZnO, were formed in the sample during the combustion process at higher ignition temperature of 623 K. The synthesized $ZnFe_2O_4$ has a sponge like porous structure and wide absorption in the visible-light region. The impurities α- Fe_2O_3 and ZnO formed in the sample probably enhance the reduction and oxidation ability and promote the separation of photo- generated electron sand holes. Comparing with $ZnFe_2O_4$ synthesized by the conventional solid state reaction, the $ZnFe_2O_4$ derived by solution combustion method showed the better photocatalytic activity under visible light radiation (Sun *et al.,* 2012).

Spinel zinc ferrite $ZnFe_2O_4$ was prepared by Sutka (2012) using co-precipitation method using the ferric chloride $FeCl_3.6H_2O$ and zinc chloride $ZnCl_2$ as raw materials and characterized by powder XRD, IR study and TG-DSC analysis. The influence of ferrite synthesis condition, such as Zn/Fe molar ratio, pH value and time was investigated. The results show that the pure spinel ferrite

$ZnFe_2O_4$ are formed when the Zn/Fe molar ratio as 1:2 at pH = 7.5 and product was calcinated at 500 ^{0}C for 5 hours, the product greatly reduce the production cost (Sutka, 2012).

Magnetically recyclable $ZnFe_2O_4$/ZnO nanocomposites immobilized on different content of grapheme with favorable photocatalytic activity under solar light irradiation were successfully prepared by Sun *et al.,* (2013) on the basis of an ultrasound aided solution method. The amount of

graphene played crucial role for the photodegradation of MB under solar light irradiation, the molar ratio of $ZnFe_2O_4$ to ZnO and the content of graphene could be controlled by adjusting the amount of zinc salts and graphene oxide dispersions. The narrow band gap of $ZnFe_2O_4$ NPs and the tremendous electron transfer ability of grapheme sheets were both in favor of the photocatalysis procedure. The most excellent photocatalytic activity under solar light irradiation was displayed when the molar ratio of $ZnFe_2O_4$ to ZnO was 0.1 and the weight ratio of graphene to $ZnFe_2O_4$/ZnO was 0.04. Furthermore, the novel photocatalyst could be conveniently separated and recycled by an external magnetic field due to its high magnetism (Sun *et al.*, 2013).

Manikandan *et al.*, (2013) prepared nanocrystalline pure and Mg-doped $ZnFe_2O_4$ ($Zn1_xMgxFe_2O_4$ with x = 0.0, 0.1, 0.2, 0.3 0.4, 0.5, 0.6, 0.7 and 0.8) samples using microwave combustion method using urea as the fuel. The average particle size obtained were of 15–43 nm.

The obtained samples were characterized by powder X-Ray Diffraction (XRD), High Resolution Scanning Electron Microscopy (HR-SEM), energy dispersive X-ray analysis, UV–Visible Diffuse

Reflectance Spectra (DRS), Photo-Luminescence (PL) spectra and Vibrating Sample Magnetometer (VSM). XRD results confirm the formation of cubic spinel-type structure with an average crystallite size in the range of 15–43 nm. Lattice parameter decreases with increasing Mg concentration, due to the smaller ionic radius of Mg2+ ion. The HR-SEM images show the morphology of the samples as spherical shaped particles in agglomeration. The broad visible emission band is observed in the entire PL spectrum. The estimated band gap energy is found to decrease with increasing Mg content (2.15–1.4eV). The magnetization showed an increasing trend with increasing Mg concentration (x = 0.5), due to the rearrangement of cations at tetrahedral and octahedral sites. Thus, it can be concluded that the different changes occur in the

properties of Mg doped Zn-ferrite nanoparticles is due to the rearrangements of divalent metal cations at different lattice sites (Manikandan *et al.*, 2013).

Nanoparticles (NPs) and Colloidal Nanocrystal Clusters (CNCs) of $ZnFe_2O_4$ were synthesized by using a solvothermal method in a controlled manner through simply adjusting the solvents. When a glycerol/water mixture was used as the solvent, $ZnFe_2O_4$ NPs were obtained. However, using ethylene glycol solvent yielded well-dispersed $ZnFe_2O_4$ CNCs. XRD and Transmission Electron Microscopy (TEM) data confirmed that the $ZnFe_2O_4$ NPs were a single crystalline phase with tunable sizes ranging from 12 to 20 nm, while the $ZnFe_2O_4$ CNCs of submicrometer size consisted of single-crystalline nano sheets. Magnetic measurement results showed that the NPs were ferromagnetic with a very small hysteresis loop at room temperature. However, CNCs displayed a super paramagnetic behavior due to preferred orientations of the nanosheets. Electrochemical sensing properties showed that both the size of the NPs and the structure of the CNCs had a great influence on their electrochemical properties in the reduction of H_2O_2. These results presented in this paper are helpful for the controlled synthesis of targeted magnetic nanomaterials by rational design (Guo *et al.*, 2013).

Nanostructured zinc ferrites with different excess iron contents ($ZnFe_2$+zO4, where z = 0.00, 0.05, 0.10 and 0.15) have been synthesized using the sol–gel auto-combustion method. The effect of excess iron on the structural, optical and visible light photocatalytic activity of zinc ferrite samples has been investigated and found that the morphology demonstrated that all of the zinc ferrite nanoparticles obtained were agglomerated together into porous clusters with the size of several microns. XRD, X-ray Photoelectron Spectroscopy (XPS), X-ray Magnetic Circular Dichroism (XMCD), Brunauer–Emmett–Teller theory, SEM, Diffuse Reflectance Spectroscopy (UV–Vis) and Photo-Luminescence Spectroscopy were used to characterize the synthesized

nonstoichiometric $ZnFe_2O_4$ powders. The XRD patterns demonstrated that the samples consist of single phase spinel structure with crystallite sizes of ~ 25 nm. SEM analysis indicated that the nanosized particles grow together in porous clusters with a size of several microns. The XPS and

XMCD analyses revealed that the excess iron ion substitutes Zn^{2+} in tetrahedral sites and in octahedral sites Fe^{2+} can be found in addition to Fe^{3+}, which could be created to restore the overall charge balance in the crystal lattice. Stoichiometric zinc ferrite ($ZnFe_2$+zO_4, z = 0.00) exhibited higher photocatalytic activity (40%) than the excess iron sample ($ZnFe_2$+zO_4, z = 0.15, i.e. 4%) under visible light irradiation for 3 h. This was explained by the formation of Fe^{2+} in the octahedral sites of excess iron $ZnFe_2O_4$; these species act as recombination centre. The stronger PL signal from the non-stoichiometric excess iron zinc ferrite samples also confirms the increasing recombination rates of photo-induced electron–hole pairs with increasing iron content. The samples showed rather broad absorption bands in a wide wavelength range from UV to visual. The band gap of (excess iron) zinc ferrite samples decreased with increasing iron content. The photocatalytic activity was lower for samples with higher iron content (Sutka *et al.*, 2012).

Feng *et al*. (2015) synthesized $ZnO/ZnFe_2O_4$ composite by a microwave combustion method using NaAc as the fuel. and shows a high adsorption capacity and high adsorption rate for the methylene blue. The obtained $ZnO/ZnFe_2O_4$ was characterized and applied for the removal of methylene blue from aquous solution in a batch system. The $ZnO/ZnFe_2O_4$ particles display larger S_{BET} and smaller size with increase of NaAc dosage. This could be as a result of certain gas being generated during NaAc decomposing and the gas prevents the particles from growing larger. Thus, the fuel has content has a significant influence on the morphologies and the adsorption capacity in microwave combustion process. More interestingly, even at neutral pH value of 7, the $ZnO/ZnFe_2O_4$ obtained with 24mL NaAc shows high rate adsorption properties with the

methylene blue removal efficiency up to 90% in 0.5min and a maximum adsorption capacity of 37.27mg/g. Thus, it can be considered that $ZnO/ZnFe_2O_4$ sorbent can be used as a promising, effective and magnetic separation adsorbent for the removal of organic dyes from waste water (Feng *et al.,* 2015).

Lee and Sharma (2015) synthesid and characterized TiO_2/NiO nanocomposites and use them as an adsorbent and a photocatalyst for naphthalene degradation in aqueous phase. TiO_2/NiO nanocomposites were synthesized by using an in-situ process for the nickel doping and further calcined at 600 ^{0}C for 6 h to produce the desired TiO2/NiO nanocomposite, which was then characterized by XPS, FTIR, XRD and UV-Vis analysis before and after naphthalene removal. The removal of naphthalene was explored with effect of pH, time and initial concentration of naphthalene (2e25 mg/L) in the presence of dark and light phases. Naphthalene removal tests were conducted under both batch and continuous flow conditions. A special column without any channeling problem was successfully designed for the removal of naphthalene by continuous flow process in the presence of visible light source. The removal was maximized at pH 6.5. The maximum amount of naphthalene removed by TiO_2/NiO (0.1) nanocomposite in the presence of visible light phase was 322.1 mg/g, which was 2.5 times greater than that of the parent TiO_2. The removal of naphthalene obtained during the breakthrough analysis was consistent with the batch equilibrium data (Lee and Sharma, 2015).

CHAPTER THREE

MATERIALS AND METHODS

3.1 Materials

The following analytical grade reagents purchased from Steeve Moore and Haddis chemical stores in Zaria, Kaduna state, Nigeria were used in this work:

i. Zinc Nitrate, $Zn(NO_3)_2.6.H_2O$ (98% purity, MW 297.48)

ii. Iron (III) nitrate, $Fe(NO_3)_3.9H_2O$ (98% purity, MW 404.00)

iii. Polyethylene glycol (98% purity, MW 1500)

iv. Sodium acetate, NaOAc (98% purity, MW 82.03)

v. Naphthalene

vi. Sodium chloride, NaCl

3.2 Apparatus

The apparatus used in this work include;

i. Conical flasks (250 and 500ml)

ii. Halogen Arc Lamp (500W), star gold

iii. Hand pipette (50ml)

iv. Measuring cylinder (100 and 200ml)

v. Plastic funnels

vi. Retort stand and G-clamps

vii. Rubber hand gloves

viii. Sample vials

ix. Spatula

x. Crucibles

xi. Stainless steel spoon

xii. Wooden Piston and mortar

3.3 Equipment

The major equipment used in this work are:

i. Digital analytical balance

ii. Magnetic stirrer

iii. Microwave oven model: 587 117, 230-240VAC, 50Hz 2450MHz, input 1150W, output 700W.

iv. UV-Vis Spectrophotometer : thermo electron~VISIONpro software V3.00, Integ.Time 00:00:01, hh:mm:ss, Lamp change 325.00 nm, Bandwidth 2.0 nm

v. Scanning Electron Microscope; PHENON PRO-X

vi. X-ray Diffractometer; X-ray tube; Cu target, 40.0 (kV) voltage and 30.0 (mA) current

3.4 Methodology

The block diagram of the research methodology is presented in Figure 3.1.

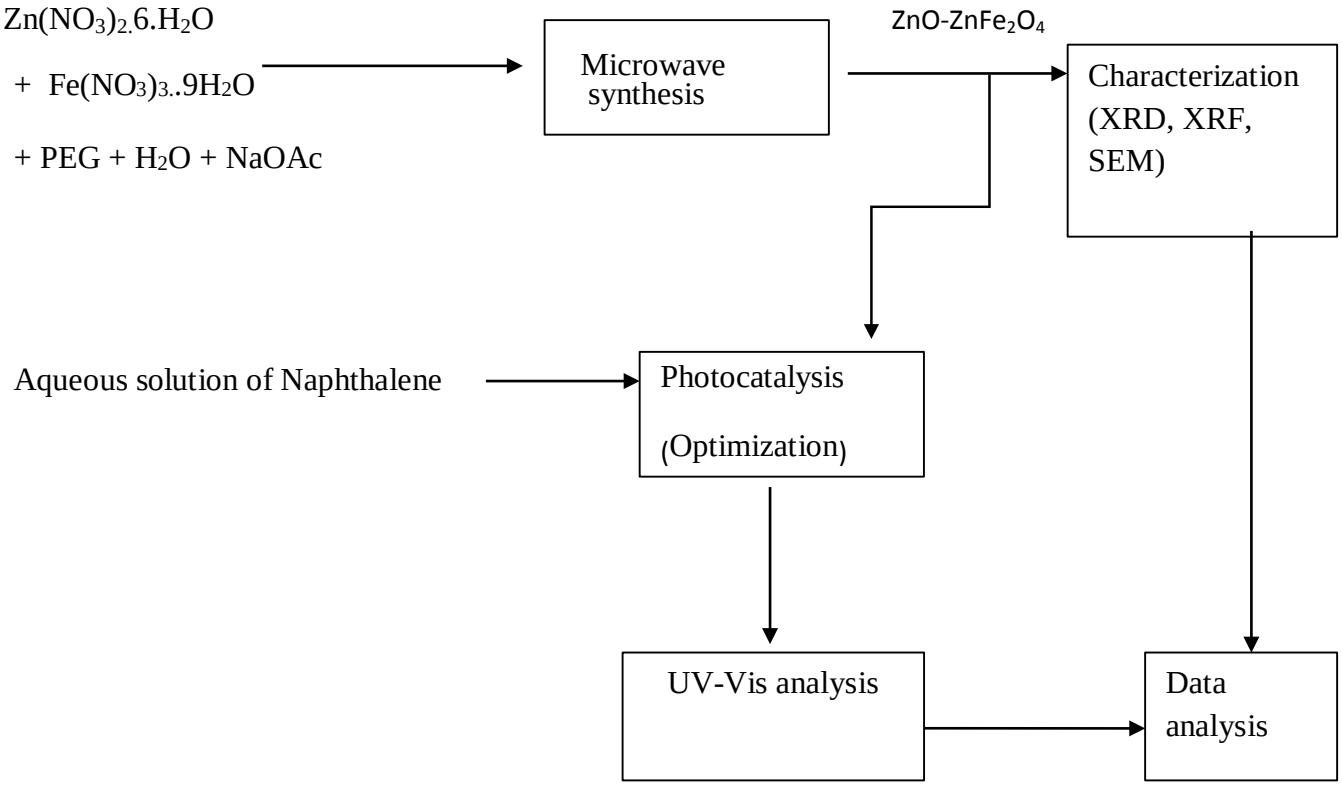


Figure 3.1: Block diagram of the research methodology

3.4.1 Microwave preparation and characterization of the ZnO-$ZnFe_2O_4$ composite

The composite preparation was carried out first with measurements of 3.3g of $Zn(NO_3)_2.6H_2O$, 0.8g of $Fe(NO_3)_3.9H_2O$ and 0.3g of polyethylene glycol with an analytical balance. The mixture was mixed vigorously and then on addition of 10ml distilled water there was a sharp color change from whitish yellow to pale yellow. And on addition of 16 ml sodium acetate, the pale yellow mixture turned brown. The mixed solution was then placed in a crucible and placed into a domestic microwave and promulgated for 5 minutes preheating and then 10 superheating. The above steps were repeated nine more times and the powder left was scrapped and collected. The

powder was then washed with 5000 ml distilled water thrice to remove undissolved salts and 1000 ml ethanol remove organic impurities. It was then allowed to settled, decanted and filtered. The filtrate was discarded and the residue was dried at 100 ^{0}C for 24 hours.

The X-Ray Diffraction patterns for the synthesized ZnO-$ZnFe_2O_4$ composite was recorded with the aid of PAN analytical England Philips Diffractor meter at the National Geological Research Laboratory Barnawa Kaduna with measurement conditions of X-ray tube; Cu target, 40.0 (kV) voltage and 30.0 (mA) current. Slits; 1.00000 (deg) divergence slit, 1.00000 (deg) scatter slit, 0.30000 (mm) receiving slit. Scanning was done at Theta-2Theta drive axis, 5.000 - 65.000 scan range, Continuous scan mode, 5.0000 (deg/min) scan speed, 0.0200 (deg) sampling pitch and 0.24 (sec) preset time. Both oxide and elemental chemical composition of the synthesized composite were obtained using PAN analytical England Philips Diffractor meter at the Defence Industry Corporation of Nigeria (DICON) at 15kV acceleration voltage and 10nA beam current. Scanning Electron Microscopy of the synthesized catalyst was determined using a PHENON PROX microscope at the Chemical Engineering Department, Ahmadu Bello University, Zaria.

3.4.2 Photocatalytic degradation of naphthalene using ZnO-$ZnFe_2O_4$ composite

Aqueous solutions of naphthalene of varying concentrations were prepared by serial dilution method. The salinity of some of the solutions was altered by dissolving appropriate amount of NaCl in the solutions. A 500 W halogen tungsten lamp was used as the source of visible light irradiation. A pre-determined amount of the synthesized ZnO-$ZnFe_2O_4$ powders were dispersed into 100 ml of naphthalene solution in the photoreactor at room temperature. Before irradiation, the suspensions were stirred for 60 mins in the dark to ensure that the naphthalene molecules could reach adsorption/desorption equilibrium on the photocatalyst surface. The stirred

suspensions were continuously irradiated for another 60 mins, after which, the $ZnO\text{-}ZnFe_2O_4$ powders particles were filtered. The residual concentration of naphthalene was measured using the UV–Vis spectrometer at 275 nm (the maximum absorption wavelength of naphthalene).

$$Degradation\,\% = 100x\left[\frac{A_0 - A}{A_0}\right] \ldots\ldots\ldots\ldots\ldots\ldots\ldots\ldots\ldots\ldots\ldots\ldots\ldots\ldots\ldots\ldots\ldots\ldots\ldots\ldots\ldots\ldots\ldots\ldots..3.1$$

where; A_0 and A are absorbance of blank and sample, respectively.

Design of experiments is a systematic approach for determining the importance of process variables, their interaction, and controlling them toward the optimum response. There are four classes of experimental designs: mixture experiments, factorial design, combined design, and response surface methodology (Wagner *et al.,* 2014). Response surface methodology (RSM) is applied for multivariate optimization with the minimum number of experiments. This minimizes consumption of materials and time for the experiment (Process Safety and Environmental Protection 9 9 (2 0 1 6) 120–128). The response surface can be expressed as follows:

$$y = f(x_{1,}x_{2\ldots\ldots\ldots}x_k) \ldots\ldots\ldots\ldots\ldots\ldots\ldots\ldots\ldots\ldots\ldots\ldots\ldots\ldots\ldots\ldots\ldots\ldots\ldots\ldots\ldots\ldots\ldots\ldots\ldots 3.2$$

The aim of most experiments is to optimize y. It is generally assumed that the independent variables are continuous and controllable by experiments with negligible errors. It is necessary to find an appropriate approximation for the true functional relationship between independent variables and the response surface. Second order polynomial is usually considered as a full model in RSM:

$$y = \beta_o + \sum_{i=1}^{k} \beta_i x_i + \sum_{i-1}^{k} \beta_{ii} x_i^2 + \sum \binom{k}{i=1} \sum_{i=1}^{k} \beta_{ij}\, x_i x_j + \varepsilon \ldots\ldots\ldots\ldots\ldots\ldots\ldots\ldots\ldots\ldots.3.3$$

where y is the response β_0, β_i, β_{ii}, and β_{ij} are regression coefficients, x_i is a coded independent variable, ε is the error and k is the number of factors (Process Safety and Environmental Protection

9 9 (2 0 1 6) 120–128).

The Central Composite Design (CCD) of the Response Surface Methodology (RSM) as implemented in Design Expert 6.0.6 software package was applied to study the effects of three process parameters on the photocatalytic degradation of naphthalene using the synthesized $ZnOZnFe_2O_4$ composite. The RSM provides insight into the interactions among the investigated process parameters and their influence on the response (degradation of naphthalene after 60 min of photocatalytic treatment, in %,). The RSM is also useful in optimization of the process conditions. A three-factorial CCD of the RSM was used. Twenty experiments were designed. The designed experiments consist of 8 factorial points, 6 axial points, and 6 replications at the center points in order to ascertain reproducibility of the results (Körbahti and Rauf, 2009).

The ranges of the process variables used were chosen based on published literature reports (Jing *et al.*, 2014) of the three variables. The degradation of naphthalene was obtained under the designed different experimental conditions. The experimental data were subjected to multi-way Analysis of Variance (ANOVA) to determine the significance of the model equation and the process parameters (initial concentration of naphthalene, $ZnO\text{-}ZnFe_2O_4$ dosage and salinity). An empirical model describing the photocatalytic process was developed for predicting the photocatalytic degradation of naphthalene and determination of optimal conditions for on the photocatalytic degradation of naphthalene using the synthesized $ZnO\text{-}ZnFe_2O_4$ composite. The experimental degradations of naphthalene were fitted to the second-order polynomial equation using a multiple regression technique.

Table 3.1: Design Summary including actual values of the uncoded factors for the photocatalytic degradation of naphthalene using the synthesized ZnO-$ZnFe_2O_4$ composite

Variable	Symbol	Unit	Low actual	High actual
Initial concentration of naphthalene	A	mg/l	5.00	25.00 (Jing et.al.,2014)
Photocatalyst (ZnO-$ZnFe_2O_4$) dosage	B	g/l	0.50	2.50 (Muneer et.al.,2012)
Salinity	C	ppt	0.00	35.00 (Patrick, 2006)

CHAPTER FOUR

RESULTS AND DISCUSSION

The chapter presents and discusses the measured properties of the synthesized ZnO-$ZnFe_2O_4$ composite. The obtained experimental and modeling results are also presented and discussed in this chapter.

4.1 Characterization of the Synthesized ZnO-$ZnFe_2O_4$ Composite

4.1.1 Chemical Composition of the ZnO-$ZnFe_2O_4$ composite

Table 4.1: Chemical composition of the ZnO-$ZnFe_2O_4$ composite

Component	Composition (% wt.)
SiO_2	0.43%
P_2O_5	0.42%
SO_3	4.93%
CaO	0.21%
Cr_2O_3	0.04%
MnO	0.01%
Fe_2O_3	**13.56%**
CuO	0.03%
ZnO	**79.94%**
La_2O_3	0.13%
Eu_2O_3	0.14%
Yb_2O_3	0.15%

The XRF result presented in Table 4.1 indicates that the main components of the composite are ZnO (79.94%) and Fe_2O_3 (13.56%). When converted into molar ratio form, the molar ratio of Fe to Zn was to be 0.16, which is close to our designed value of 0.18.

4.1.2 XRD Analysis of the ZnO-$ZnFe_2O_4$ composite

In order to determine the crystalline phases present in the ZnO-$ZnFe_2O_4$ Composite, the X-ray powder diffraction was used. The XRD pattern presented in Figure 4.1 features a set of peaks at Bragg angles of 31.6, 34.4, 36.2, 47.6, 56.6, 68.8 and 72.6° due to ZnO (JCPDS36-1451), and another set of relatively weaker peaks at 29.9, 35.2, 42.7, 53.2 and 62.20° that correspond to standard XRD data of $ZnFe_2O_4$ (JCPDS22-1012). The broadness of the diffraction peaks is due to very small sizes of the crystals. The broadness of the peaks also indicates that the synthesized

ZnO-$ZnFe_2O_4$ composite has very low crystallite sizes.

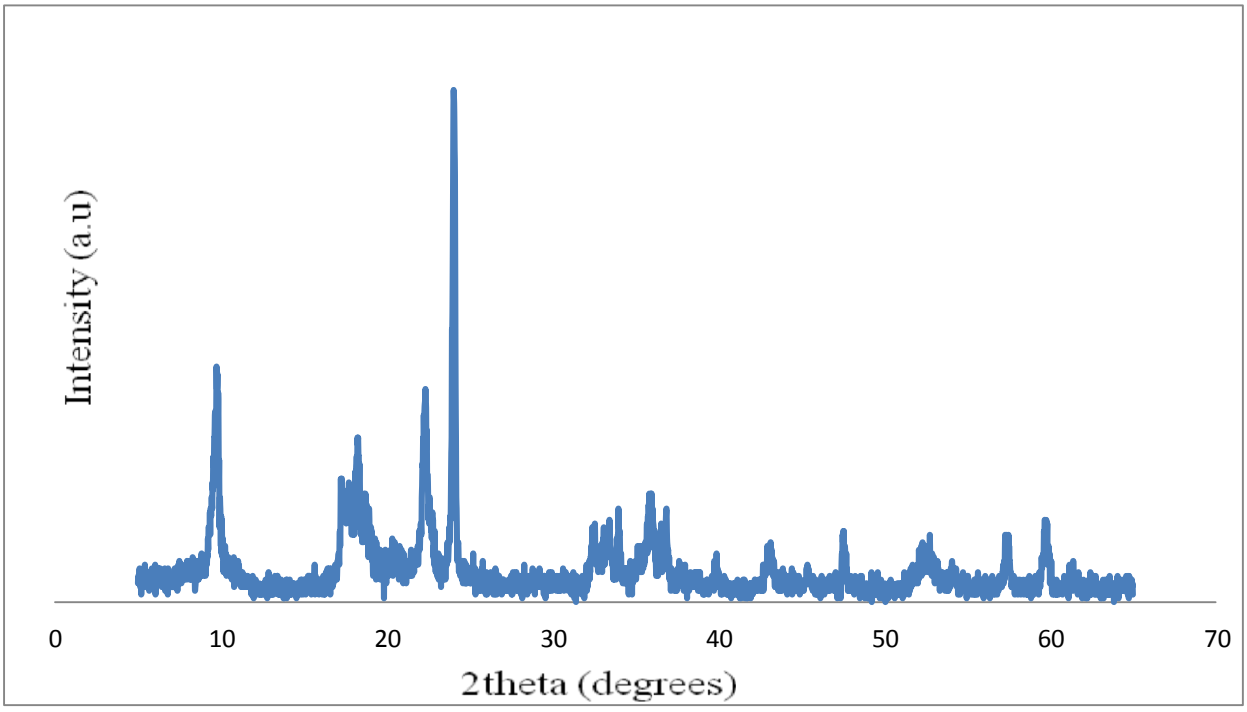


Figure 4.1: XRD pattern of the ZnO-$ZnFe_2O_4$ Composite

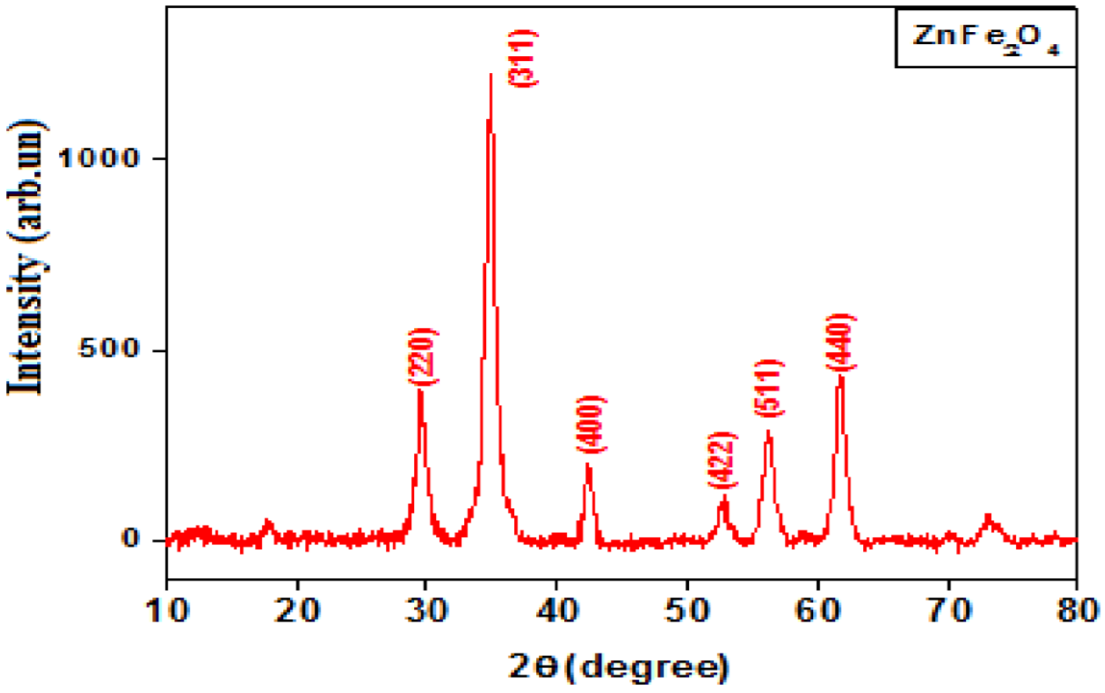


Figure 4.2: XRD pattern of $ZnFe_2O_4$ (www.intechopen.com accessed 6/7/2016)

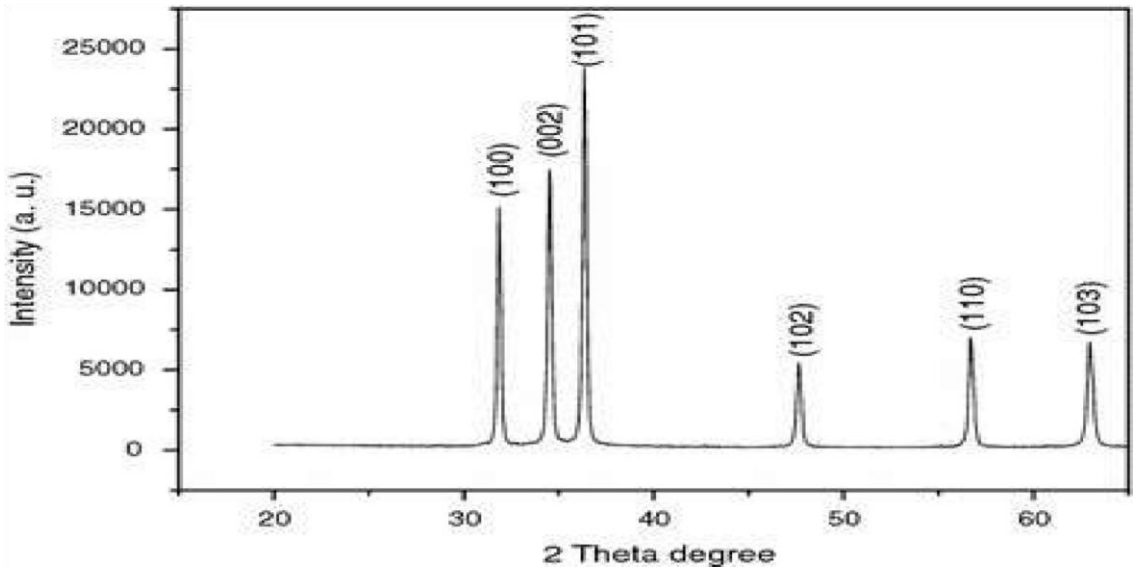


Figure 4.3: XRD pattern of ZnO (www.researchgate.net accessed 6/7/2016)

4.1.3 SEM Analysis of the Developed ZnO-$ZnFe_2O_4$ Photocatalyst

The SEM presented in Plate 4.1 reveals that the ZnO-$ZnFe_2O_4$ composite is uniformly dispersed. The composite is highly porous material. This high porosity can be attributed to the rapid release of gases during the microwave synthesis (Feng *et al.,* 2015). The high porosity enhances the specific surface area of the composite which in turn will increase substrate adsorption onto the composite and subsequent photocatalytic degradation of the substrate. The porosity of the ZnO-

$ZnFe_2O_4$ also helps it to trap light and to be more efficiently activated by the light

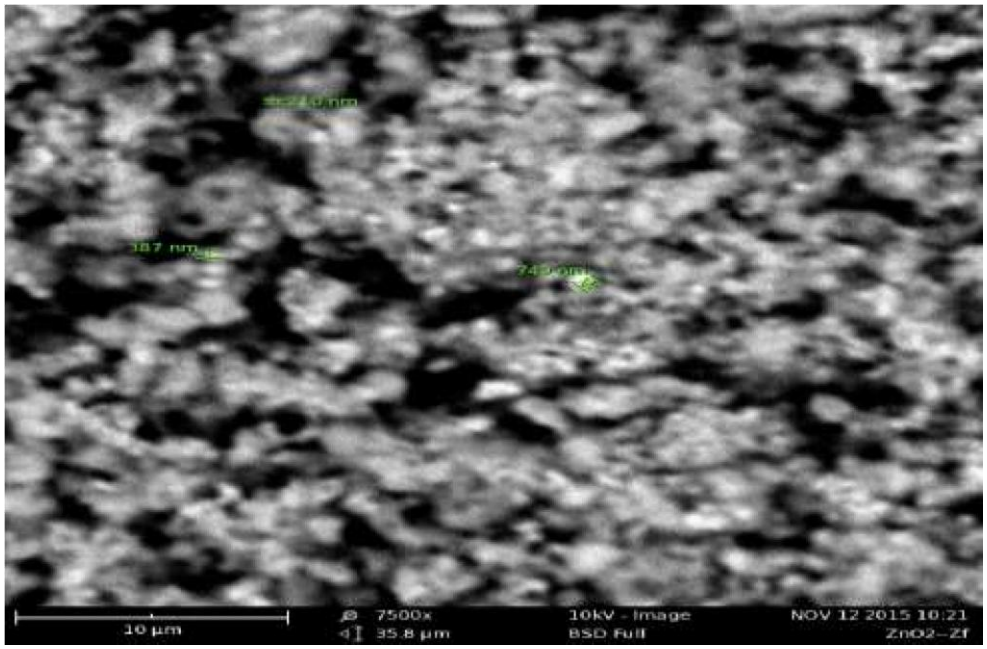


Plate 4.1: Scanning electron microscopic image of the ZnO-$ZnFe_2O_4$ composite

4.2 Photocatalytic degradation of naphthalene using the synthesized ZnO-$ZnFe_2O_4$ composite.

Control experiment was carried out in the dark in order to serve as the control for the photocatalytic degradation experiment. Thus, 100ml a suspension of naphthalene with initial concentration of 16.8mg/l and 0.05 g of ZnO-$ZnFe_2O_4$ was stirred in the dark for 60 mins. The results indicate that only 46.6 % of naphthalene was removed via adsorption on the surface of the ZnO-$ZnFe_2O_4$ composite. However, when the same experiment was carried out under visible light irradiation, 99.04% of naphthalene was degraded via photocatalysis. Hence, photocatalysis is very efficient in naphthalene degradation. The following subsections (4.2.1 and 4.2.2) presents and discusses the results of modeling and optimization of photocatalytic degradation of naphthalene using the synthesized ZnO-$ZnFe_2O_4$ composite.

4.2.1 Modeling of photocatalytic degradation of naphthalene using the synthesized ZnO-$ZnFe_2O_4$ composite

The effect of three process parameters (ZnO-$ZnFe_2O_4$ dosage, initial concentration of naphthalene and salinity) on the percentage photocatalytic degradation of naphthalene were analyzed using the CCD based on the RSM. The design matrix consisting of the three process variables, experimental and predicted values of the percentage degradation of naphthalene is presented in Table 4.2. The experimental responses were used to develop model equation that describes photocatalytic degradation of naphthalene using the synthesized ZnO-$ZnFe_2O_4$ composite.

Table 4.2 shows various model equations that were predicted by the Design Expert 6.0.6. Software. As apparent in Table 4.2, the design expert software suggested quadratic model by checking the adequacy of various mathematical models using ANOVA.

Table 4.2: Design matrix for the photocatalytic degradation of naphthalene using the synthesized ZnO-$ZnFe_2O_4$ composite, experimental conditions and results of CCD model

RUN	Actual variables			Degradation, (%)		Difference between X and Y
	A	B	C	Experimental X	Predicted Y	
1	1.8	150.0	17.5	52.6	51.2	-1.4
2	15.0	18.2	17.5	94.6	94.5	-0.1
3	5.0	50.0	0.0	76.9	79.9	3
4	15.0	150.0	17.5	52.2	53.2	1
5	5.0	50.0	35.0	83.6	86.1	2.5
6	15.0	150.0	17.5	52.3	53.2	0.9
7	15.0	150.0	46.9	52.8	58.5	5.7
8	15.0	150.0	11.9	52.3	52.2	-0.1
9	25.0	50.0	0.0	85.5	82.9	-2.6
10	15.0	150.0	17.5	52.7	53.2	0.5
11	15.0	150.0	17.5	53.5	53.2	-0.3
12	15.0	150.0	17.5	49.2	53.2	4
13	31.8	150.0	17.5	50.7	55.7	5
14	5.0	250.0	0.0	21.0	17.2	-3.8
15	25.0	250.0	0.0	18.7	20.3	1.6
16	15.0	150.0	17.5	49.6	53.2	3.6
17	15.0	318.2	17.5	58.3	58.5	0.2
18	25.0	250.0	35.0	21.3	26.5	5.2
19	5.0	250.0	35.0	22.5	23.5	1
20	25.0	50.0	35.0	68.9	89.2	20.3

The large difference between the predicted and experimental values in Table 4.2, run 20 could be as a result of human errors encountered during which the experiment was conducted in that particular run. The high F-value (333.26) of quadratic model indicates that the model is significant.

The value of "Prob > F" for the quadratic model (<0.0001) is less than 0.0500; this also indicates that the quadratic model is significant. The values of R^2 provide a measure of how much variability in the observed response values can be explained by the experimental factors and their interactions. The value of R^2 is always between 0 and 1. The closer the R^2 value is to 1, the stronger the model is and the better it predicts the response. The R^2 value of 0.9993 is in reasonable agreement with the adjusted R^2 of 0.9985. The adjusted R^2 corrects the R^2 value for the sample size and the number of terms in the model. If there are many terms in the model and the sample size is not very large, the adjusted R^2 may be noticeably smaller than the R^2. In other words, adding a variable to the model could always increase R^2, regardless of whether the additional variables are statistically significant. Hence, it is preferable to use adjusted- R^2. When variables are added to the model, the adjusted- R^2 will not necessarily increase. If unnecessary variables are R^2 and adjusted- R^2 means that insignificant variables are included in the model. Adeq Precision measures the signal to noise ratio. A ratio greater than 4 is desirable. In this case, a ratio of 122.795 indicates an adequate signal. Hence, the developed model can be used to navigate the design space.The value of "Prob > F" for the Lack-of-Fit of the quadratic model (0.083) is an indication that the Lack-of-Fit is insignificant relative to the pure error.

The developed model quadratic equation is given by:

$$\boldsymbol{Degradation}\ (\%) = \mathbf{103.128} + \mathbf{0.112}\,\boldsymbol{A} - \mathbf{0.084}\boldsymbol{B} - \mathbf{0.175}\boldsymbol{C} - \mathbf{0.008}\boldsymbol{A^2} - \mathbf{0.001}\boldsymbol{B^2} - \mathbf{0.008}\boldsymbol{C^2} + \mathbf{0.003}\boldsymbol{AB} - \mathbf{0.002}\boldsymbol{AC} + \mathbf{0.002}\boldsymbol{BC} \quad \textbf{.....4.1}$$

The developed model terms were subjected to ANOVA using the Design expert 6.0.6 software package. From the ANOVA results in Table 4.3, the statistical significance of the model and each model term, as well as the quality of the fit of the quadratic model were determined at 5% significance level (95% confidence interval). The F values and values of Prob > F were used as a tool to check the significance of each of the coefficients. The smaller the Prob > F value, the more significant is the corresponding coefficient. The Prob > F values suggest that, among the three variables, ZnO-$ZnFe_2O_4$ dosage and initial concentration of naphthalene have the largest effect on degradation process. The linear and quadratic relations between ZnO-$ZnFe_2O_4$ dosage and initial concentration of naphthalene, as well as the linear and quadratic relations between ZnO-$ZnFe_2O_4$ dosage and salinity are also highly significant ($p < 0.05$).

Table 4.3: ANOVA for the developed model quadratic equation describing photocatalytic degradation of naphthalene using the $ZnO\text{-}ZnFe_2O_4$ composite

Source	Sum of Squares	DF	Mean Square	F Value	Prob > F
Model	5313.37	9	590.37	1176.69	< 0.0001 significant
A	67.42	1	67.42	134.38	< 0.0001 significant
B	3559.61	1	3559.61	7094.77	< 0.0001 significant
C	1.73	1	1.73	3.45	0.1056 not significant
A2	8.42	1	8.42	16.77	0.0046 significant
B2	489.78	1	489.78	976.21	< 0.0001 significant
C2	3.95	1	3.95	7.87	0.0263 significant
AB	33.31	1	33.31	66.39	< 0.0001 significant
AC	0.69	1	0.69	1.37	0.2798 not significant
BC	29.57	1	29.57	58.95	0.0001 significant
Residual	3.51	7	0.50		
Lack of Fit	2.22	2	1.11	4.29	0.0823 not significant

Response surface plots and contour diagrams help in identification of the type of interactions between the investigated process variables. Each contour curve represents an infinite number of combinations of two tested variables with the other two maintained at their respective zero level. A circular contour of response surfaces indicates that the interaction between the corresponding variables is negligible. In contrast, an elliptical or saddle nature of the contour plots indicates that the interaction between the corresponding variables is significant. The response surface and contour plots for the effect of each pair of the studied variables are shown in Figure 4.4 to 4.6.

The degradation rate decreases with increase in the ZnO-$ZnFe_2O_4$ dosage. The number of active sites increases with increase in ZnO-$ZnFe_2O_4$ dosage; however, light penetration, and hence, the photoactivated volume of the suspension shrinks at high ZnO-$ZnFe_2O_4$ dosage. This is due to increased opacity of the suspension and also increased light reflectance as a consequence of surplus photocatalyst particles. In addition, deactivation of the activated molecules by collision with ground state molecules, and shielding by the photocatalyst particles and agglomeration and sedimentation of the photocatalyst particles may also contributed to decreased percentage of degradation at the range of the ZnO-$ZnFe_2O_4$ dosage used. Similar observations by Noureddine et al., 2015, Revanasiddappa and Khezrianjoo 2012, and Beata, 2008 have also been reported in other studies on other organic substrates. There is strong interaction between the initial concentration of naphthalene and ZnO-$ZnFe_2O_4$ dosage especially at high ZnO-$ZnFe_2O_4$ dosages. Degradation of naphthalene increases with increase in initial concentration of naphthalene. Noureddine et al., 2015, Revanasiddappa and Khezrianjoo 2012, and Beata, 2008 have shown that with increase in substrate concentration, more molecules of the substrate are adsorbed onto the photocatalyst surface, and this will lead to improve photocatalytic degradation of the substrate (Process Safety and Environmental Protection 9 9 (2 0 1 6) 120–128). As shown in Figure 4.5 and 4.6, salinity doesn't have significant effect on the photocatalytic process. This can also be seen from the ANOVA presented in Table 4.2. Percentage degradation of naphthalene decreases with increase in the salinity. Indeed, Jing *et al*. (2014) reported that salinity impedes photolytic degradation of naphthalene because of the existence of free-radical scavengers and photon competitors. Figures 4.4-4.6 show the strong interactions between salinity and initial concentration of naphthalene, and the ZnO-$ZnFe_2O_4$ dosage. The highest photocatalytic

degradation of naphthalene is achieved at salinity of zero (that is in fresh water).

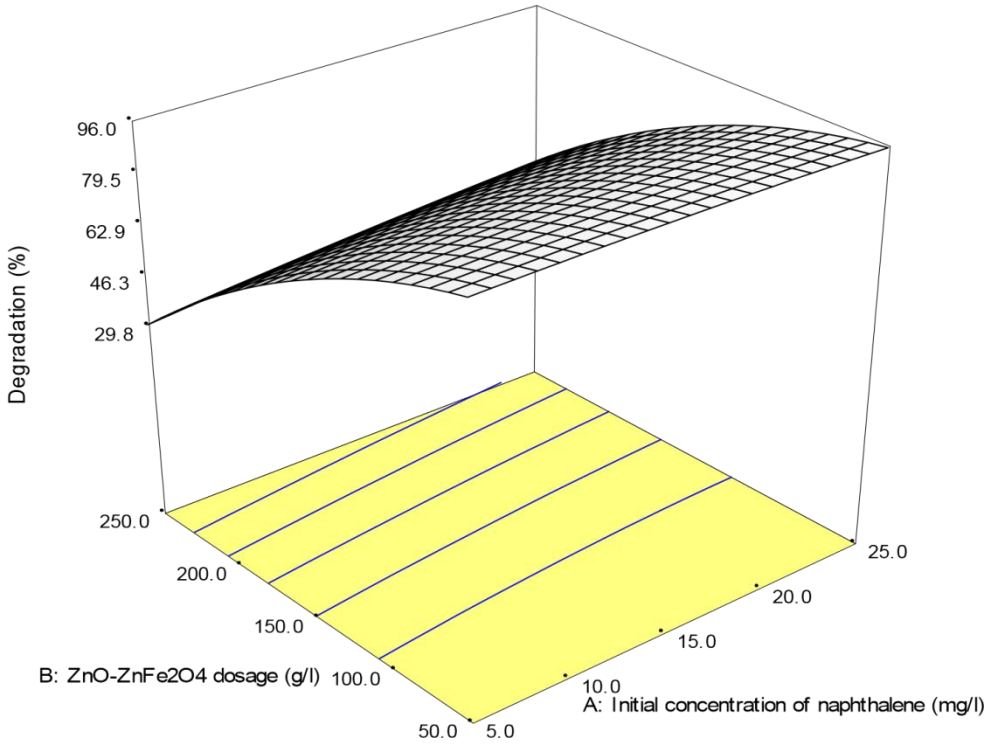


Figure 4.4. Response surface for simultaneous influence of initial concentration of naphthalene and $ZnO\text{-}ZnFe_2O_4$ dosage

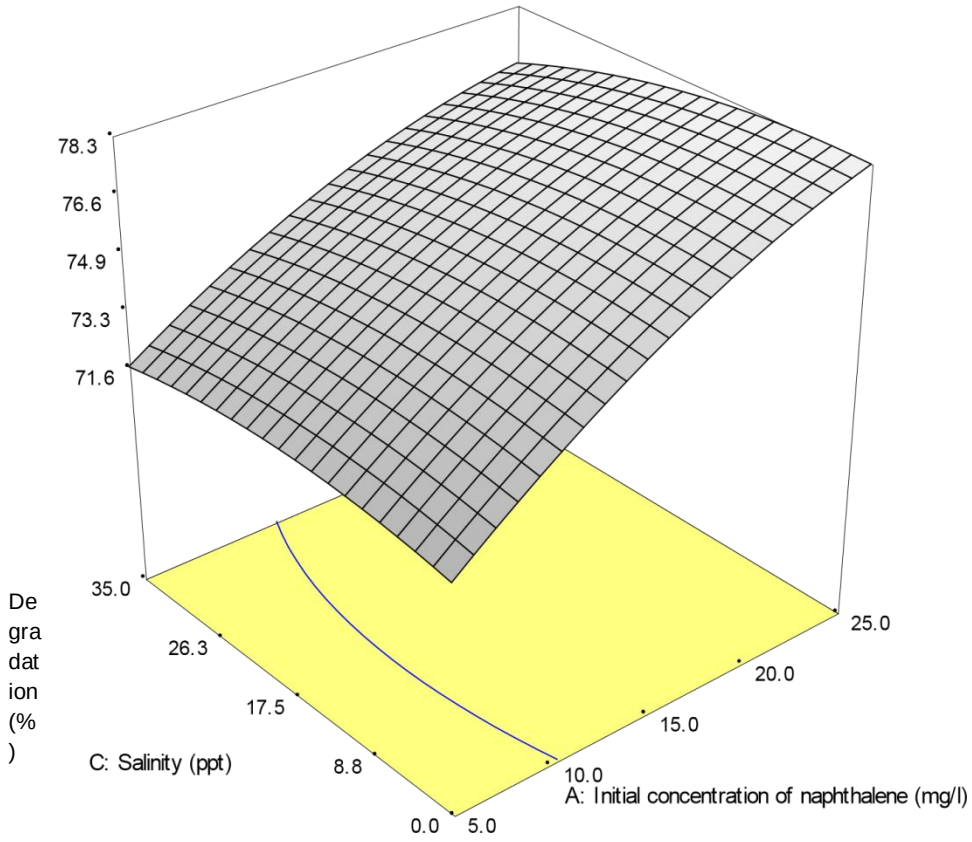


Figure 4.5. Response surface for simultaneous influence of initial concentration of naphthalene and salinity

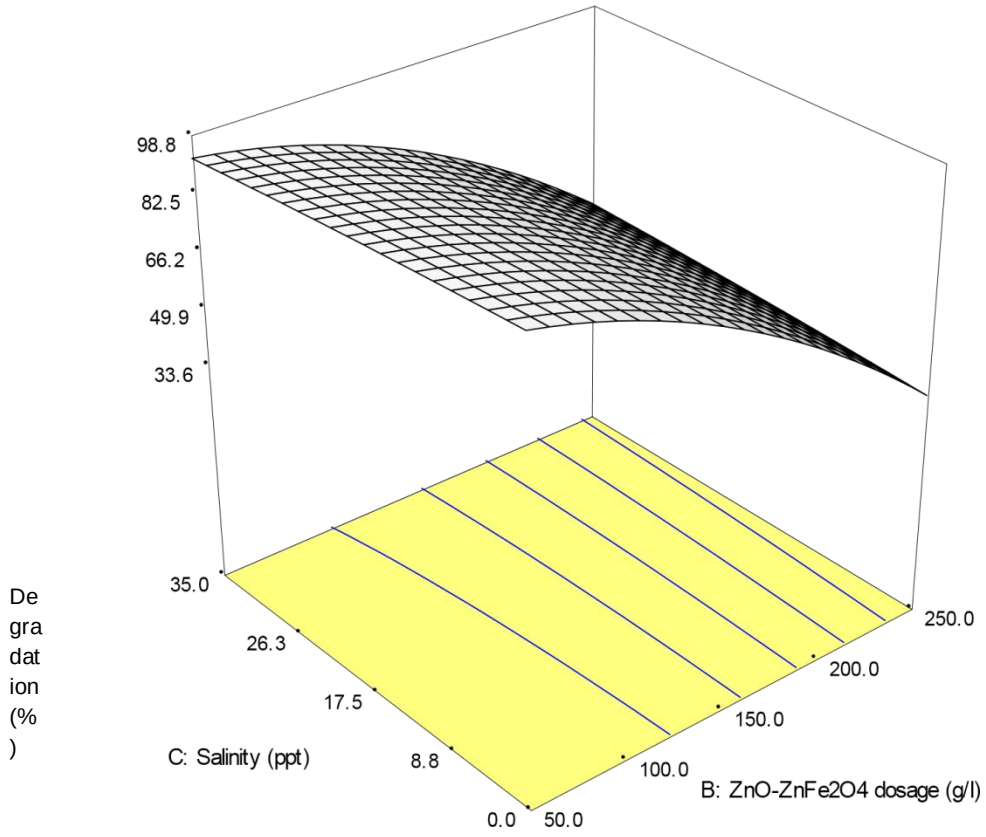


Figure 4.6: Response surface for simultaneous influence of ZnO-$ZnFe_2O_4$ dosage and salinity

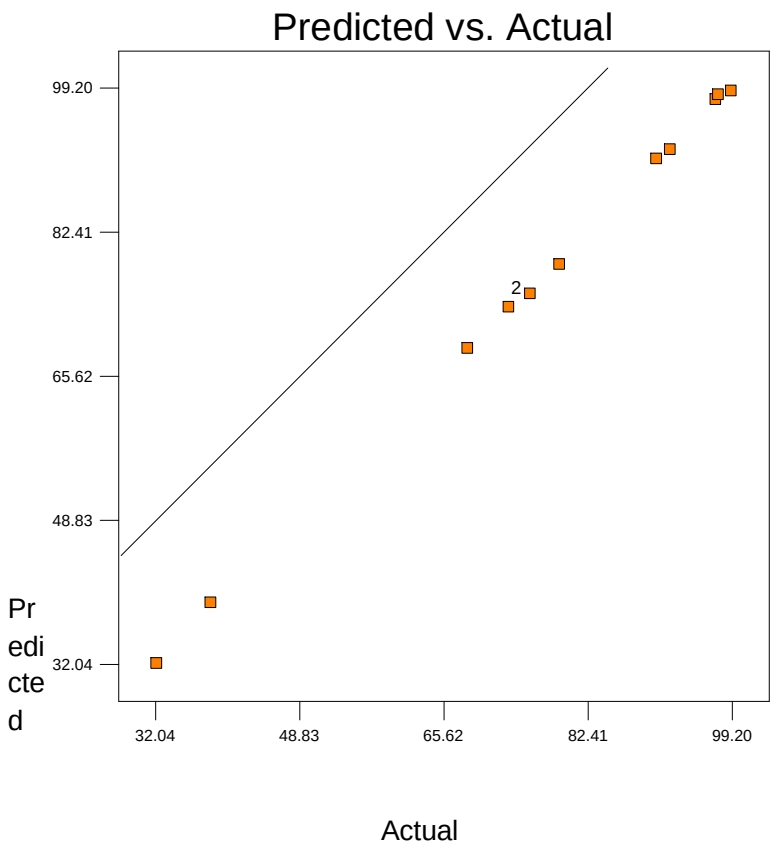


Figure 4.7: Plot of predicted values against actual values

As presented in Table 4.2, under the designed experimental conditions, the highest and lowest degradation of naphthalene achieved are 99.2% and 32.3%, respectively. The experimental and predicted values of the percentage degradation of naphthalene are very close. This can also be seen from the plot of actual versus predicted values displayed in Figure 4. 7. This implies that the quadratic model explains perfectly the experimental range studied.

Figure 4.8 shows normal plot of residuals, normal percentile probability against residuals. From where it is seen that all the errors encountered during and after which the experiment was conducted follow a particular pattern that have not deviate from the approved normal probability plot of residuals theory.

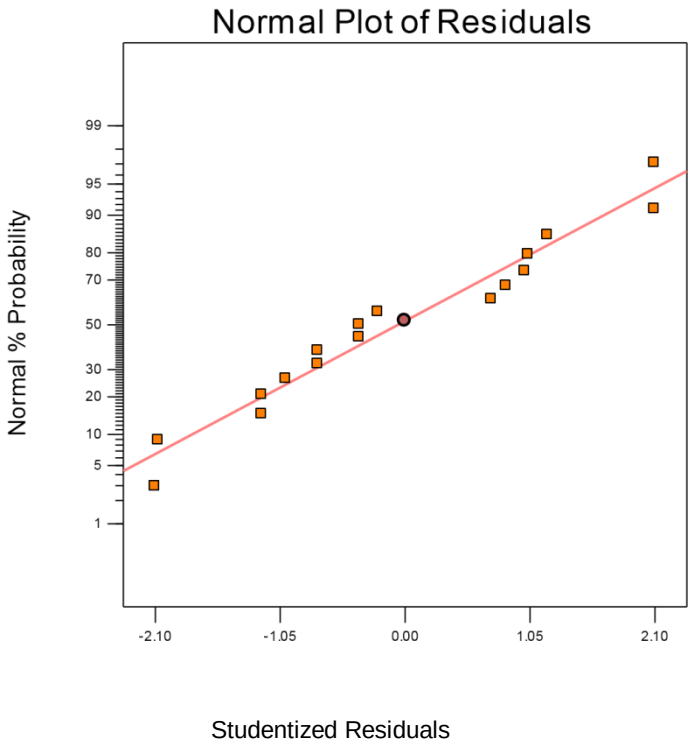


Figure 4.8: Normal plot of residuals, normal percentile probability against residuals

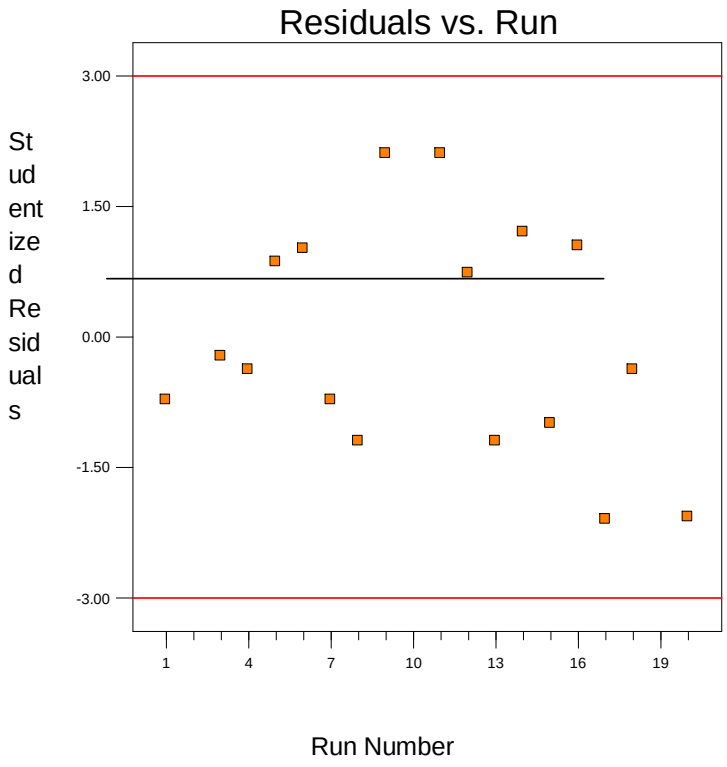


Figure 4.9. Residual versus run plot

A good plot of residual versus run number should be a random scatter that is, not follow a particular trend or pattern. Following a particular pattern indicates a problem with the model, a possible transformation or a special cause that merits ignoring the results of the runs. The random scatter found in Figures 4.9 indicates that the model is good and should not be discarded.

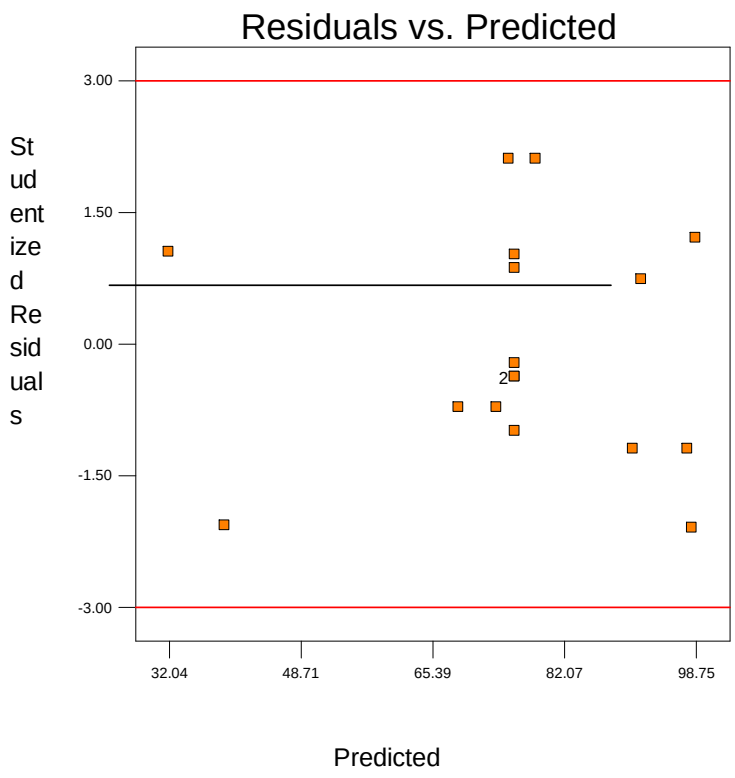


Figure 4.10: Residual versus predicted plot

The residual by predicted plot is normally used in diagnosing nonlinearity or non-constant error variance. It is usually used in finding outliers. A good predicted result shows a random scatter as shown in Figure 4.10, not a particular pattern.

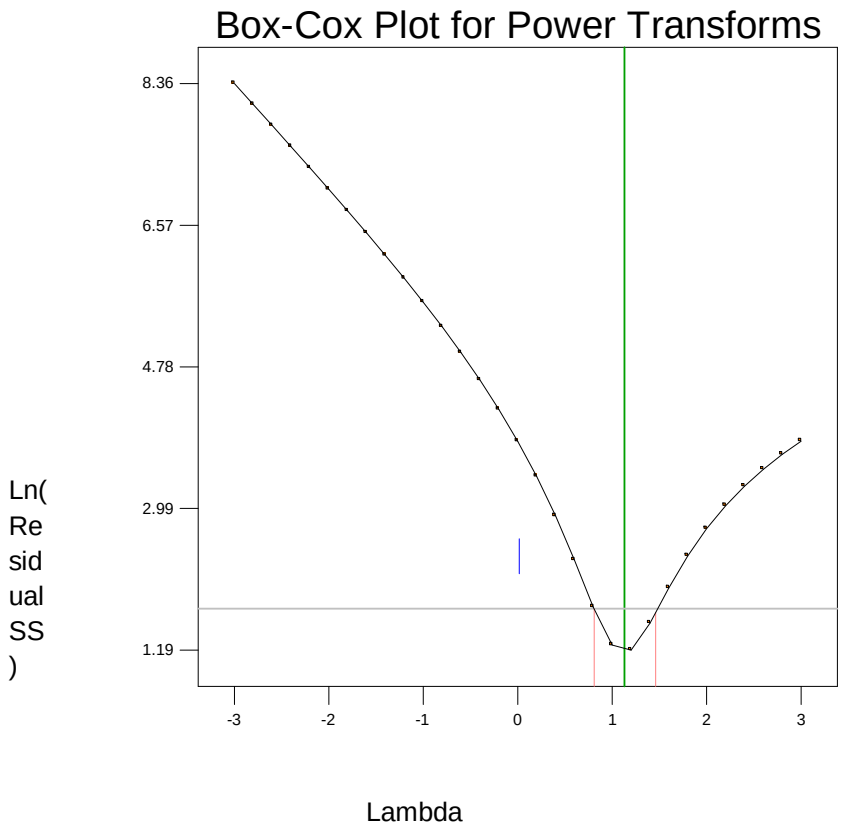


Figure 4.11: Box-Cox plot for power transforms of photo degradation

The Box-Cox plot is used in determining whether a power law transformation may be appropriate for the data. The blue line indicates the current transformation, the green line indicates the best lambda and the red line indicates 95% confidence interval associated with the best lambda value. In Figure 4.11, the current lambda is 1 and the best lambda is 1.49. The confidence interval includes 1 and thus the recommendation for standard transformation like log for instance is none. This means that there is absolutely no need for power law transformation to improve the given data for other statistical tools to be employed in analyzing the data.

4.2.2 Optimization of photocatalytic degradation of naphthalene using the synthesized $ZnO\text{-}ZnFe_2O_4$ composite

To determine the optimum values of the three process variables amount that will lead to the highest photocatalytic degradation of naphthalene, optimization of the variables was performed using the numerical method of Design expert 6.0.6. The desirable goal was to achieve maximum photocatalytic degradation of phenol; whereas, the three process variables were placed within the range of their experimental values studied. Table 4.6 presents the solutions of the numerical optimization for degradation of naphthalene. The selected optimization solution predicted maximum percentage degradation of 98.8% under the predicted optimum conditions of initial naphthalene concentration of 16.8mg/L, $ZnO\text{-}ZnFe_2O_4$ dosage of 0.50 g/L, and salinity of 0 ppt.

To validate the developed quadratic model for predicting the optimum values of process variables of photocatalytic degradation of naphthalene, an additional experiment was performed under the predicted optimum conditions listed in Table 4.4. The experimental and the predicted values of naphthalene degradation under the predicted optimum values are presented in Table 4.4. It can be seen that the experimental degradation (98.8 %) is in excellent agreement with the predicted degradation (99.04 %). This verifies the model validation. Therefore, the developed quadratic model is reliable for predicting photocatalytic degradation of naphthalene.

.

Table 4.4. Experimental and predicted values of naphthalene degradation under the predicted optimum values of the process variables

Process variables	Optimum conditions	Degradation (%)	
		Experimental	Predicted
Initial concentration of naphthalene (mg/L)	16.8	98.8	99.04
$ZnO\text{-}ZnFe_2O_4$ dosage (g/L)	0.5		
Salinity (ppt)	0.0		

It is instructive to compare the present results with some recent literature reports on modeling and optimization of photocatalytic degradation of naphthalene using various catalysts. Mahmoodi and Sargolzaei, (2014) applied the RSM to model and optimize photocatalytic degradation of naphthalene using TiO_2 nanoparticles as the photocatalyst. They developed a quadratic model that described the effect of the four independent parameters (agitation speed, air flow rate, photocatalyst dosage, and UV light intensity) on the degradation of naphthalene. Their optimization results showed that the maximum degradation of naphthalene can be achieved at the optimum conditions: agitation speed of 150 rpm, air flow rate of 5 L/h, TiO_2 dosage of 2.17 g/L, and UV light power of 18.67 W. Zhou *et al.*, (2012) also used RSM to model and optimize photocatalytic degradation of naphthalene using $TiO_2/Fe_3O_4\text{-}SiO_2$ as the photocatalyst under UV irradiation. Their experimental results showed that irradiation time, pH, and the photocatalyst loading had significant influence on photocatalytic degradation of naphthalene, and the maximum degradation rate of 97.39% was predicted at optimum irradiation time of 97.1 min, pH of 2.1, and

$TiO_2/Fe_3O_4\text{-}SiO_2$ dosage of 0.962 g/L, respectively. In the present work, the optimum $ZnOZnFe_2O_4$ dosage (which afforded 99.04% degradation of naphthalene under visible light irradiation) is only 0.5 g/L. Therefore, it can be concluded that the microwave synthesized $ZnOZnFe_2O_4$ composite is

more effective in photocatalytic degradation of naphthalene than TiO_2 and TiO_2/Fe_3O_4-SiO_2. It shall be noted that TiO_2 is often considered to the benchmark photocatalyst for various photocatalytic process. The high photocatalytic activity of ZnO-$ZnFe_2O_4$ under visible light irradiation makes it a very promising photocatalyst for solar driven photocataltic process because 46% of the solar spectrum is visible light; UV constitutes less than 5% of the solar spectrum (Casbeer *et al*., 2012).

CHAPTER FIVE

CONCLUSIONS AND RECOMMENDATIONS

5.1 CONCLUSIONS

i. $ZnO\text{-}ZnFe_2O_4$ composite was successful synthesized using microwave combustion method.

ii. The molar ratio of Fe to Zn in the composite is 0.16. XRD analysis shows that the synthesized $ZnO\text{-}ZnFe_2O_4$ composite is crystalline, and has very low crystallite sizes. The SEM image indicates that the $ZnO\text{-}ZnFe_2O_4$ composite is highly porous material with uniformly dispersed particles.

iii. $ZnO\text{-}ZnFe_2O_4$ dosage and initial concentration of naphthalene have the largest effect on degradation process. The highest photocatalytic degradation of naphthalene was achieved at salinity of zero (that is in fresh water) even though salinity has effect on the catalyst to some extent.

iv. Quadratic model was developed with R^2 value of 0.9993 and adjusted R^2 value of 0.9985, respectively. The predicted optimum conditions for photocatalytic degradation of naphthalene using the $ZnO\text{-}ZnFe_2O_4$ composites are: initial naphthalene concentration of 16.8mg/l, $ZnO\text{-}ZnFe_2O_4$ dosage of 0.50 g/L, and salinity of 0 ppt. The experimental and the predicted values of naphthalene degradation under the predicted optimum values are 99.04 % and 98.8 %. Hence, the developed quadratic model is reliable for predicting photocatalytic degradation of naphthalene.

5.2 RECOMMENDATIONS

i. Detailed kinetic studies of the photocatalytic degradation of naphthalene using the developed composite should be carried out.

ii. Studies on the recycling of the composites should be done.

iii. Application of the composite for the treatment of real oil spill using solar energy should be carried out. iv. Development of a floating pilot plant for the photocatalytic treatment of oil spill using the composite.

v. Detailed mineralization studies using the composite should be carried out.

REFERENCES

Abdulhahid H., Haji, A. M. and Waziri S.M., (2013), Photochemical Treatment of Tannery Effluent, *Journal of the Nigerian Society of Chemical Engineers, 0794-6759*

Beata T (2008), Increase On The Photocatalytic Activity Of Tio_2 By Carbon And Iron Modifications, *International Journal Of Photoenergy, Volume 2008*

Borse P. H., Jang J. S., Hong S. J., Lee J. S., Jung J. H., Hong T. E., Ahn C. W., Jeong E. D., Hong K. S., Yoon J. H. and Kim H. G. (2009), Photocatalytic Hydrogen Generation from Waterm ethanol Mixtures Using Nanocrystalline $ZnFe_2O_4$ under Visible Light Irradiation, *Journal of the Korean Physical Society, Vol. 55, No. 4, pp. 1472_1477*

Callister Jr W.D (2001), *Fundamentals of Material Science and Engineering,* 5th Edition, John Wiley & Sons Inc, New York, PP 154-473

Casbeer E, Sharma V.K and Li X (2012), Synthesis and photocatalytic activity of ferrites under visible light: A review, *Journal of Seperation and Purification Technology 87 1-14*

Chang R (2005), Chemistry, 8th Edition, McGraw-Hill, New York PP 930-931

Feng J, Wang Y, Zou L, Li B, He X, Ren Y, Lv Y and Fan Z (2015), Synthesis of magnetic $ZnO/ZnFe_2O_4$ by a microwave combustion method and its high rate of adsorption of methylene blue, *Journal of Colloid Interface Sci. 438 318-322*

Guo P., Cui L, Wang Y, Lv M, Wang B and Zhao X. S. (2013), Facile Synthesis of ZnFe2O4

Hamilton J.W.J, Byrne J.A., O'Shea K, Entezari M.H and Dionysiou D.D (2012), A Review of the Visible Light Active Titanium Dioxide Photocatalysts for Environmental Applications, *Journal of Applied Catalysis B:Environmental 125 331-349*

Hamilton, J.W.J, Byrne J.A., O'Shea K, Entezari M.H and Dionysiou D.D (2012), A Review Of The Visible Light Active Titaniumdioxide Photocatalyst for Environmental Applications. *Journal of Applied Catalysis B: Environmental 125 331-349*

Hossain A, Adebayo A.R and Hossain M.E (2012), A sustainable approach to controlling oil spills, *Journal of Environmental Management 133 213-227*

Irwin R.J., VanMouwerik M., Stevens L., Seese M.D and Basham W (1997), Environmental Contaminants Encyclopedia Naphthalene Entry, National Park Services, Water Resources Divisions, Colorado.

Jing L., Chen, B, Zhang B., Zheng J., and Liu.B (2014), Naphthalene Degradation in Sea water by UV Irradiation:the Effects of Fluence Rate,Salinity, Temperature and Initial Concentration.*Marine Pollution Bulletin, 81(1) 149-156*

John, I.J.,(2014), Effect of Calcination Temperature on the Composition and Photocatalytic Activity of Nigerian Natural Ilmenite, Sphalerite and Wolframite, Chemical Engineering Department, Ahmadu Bello University, Zaria.

Korbahti,B.K, and Rauf,M A (2009).Determination Of Optimum Operating Conditions Of Carmine Decoloration By Uv/H_2o_2 Using Response Surface Methodology. *Journal of Hazardous Materials,161(1),281-156*

Lan Y, Lu Y and Ren Z (2013), Mini review on photocatalysis of titaniumdioxide nanoparticles and their solar applications, *Journal of Nano Energy 2, 1031-1045*

Lee B and Sharma A (2015), Adsorptive/photo-catalytic process for naphthalene removal from aqueous media using in-situ nickel doped titanium nanocomposite, *Journal of Environmental Management 155, 114-122*

Magalhaes F, Moura F.C.C and Lago R.M (2011), TiO_2/LDPE Composite: A new floating photocatalyst for solar degradation of organic contaminants, *Desalination 276 266-271*

Mahmoodi, V., and Sargolzaei, J. (2014). Optimization of Photocatalytic Degradation of Naphthalene Using Nano-Tio_2/UV System: Statistical Analysis Using Response Surface Methodology. *Desalination and Water Treatment, 52 (34-36).6664-6672*

Malnieks K, Grinberga L and Kisand V (2014), Photocatalytic activity of non-stoichiometric ZnFe2O4 under visible light irradiation, *Physical Science 89 044011 (8pp)*

Manikandan A, Vijaya J. J, Sundararajan M, Meganathan C, Kennedy L. J and Bououdina M. (2013), Optical and magnetic properties of Mg-doped $ZnFe_2O_4$ nanoparticles prepared by rapid microwave combustion method, *Superlattices and Microstructures 64 118–131*

Moradi S, Aberoomand-Azar P, Raeis-Farshid S, Abedini-Khorrami S and Givianrad M.H (2012), The effect of different molar ratios of ZnO on characterization and photocatalytic activity of TiO_2/ZnO nanocomposite, *Journal of Saudi Chemical Society*

Muneer M.B, Abdul A.H.K, Abubakar M, Mohd S.T and Kamaruzzman S (2012), Photocatalytic Degradation of Chlorophenols under Direct Solar Radiation in the Presence of Zno Catalyst, *Research on Chemical Intermediates, volume 39, pp 1981-1996*

Nanoparticles with Tunable Magnetic and Sensing Properties, *Langmuir 29, 8997−9003*

Noureddine B, Idriss B, Samir Q, Ali A and Yhya A (2015), Degradation of Phenol in Water by Titanium Dioxide Photocatalysis, *Oriental Journal Of Chemistry, volume 29 Number 3*

Nwilo P. C. and Badejo O. T., Impacts and Management of Oil Spill Pollution along the Nigerian Coastal Areas,

Patrick D.B (2006), Measuring the Effects of Salinity Stress in the Red Mangrove, Rhizophora mangle L., African Journal of Agricultural Research vol.1 (1), pp 001-004

Pelaez M, Nolan N.T, Pillai S.C, Seery M.K, Falaras P, Kontos A. G, Dunlop P.S.M, Hamilton

Potter T.L and Simmons K.E .,(1998), Composition of Petroleum Mixtures: Amherst, Mass., Amherst Scientific Publishers, Total Petroleum Hydrocarbon Criteria Working Group Series, v.2, 102 p.

Revanasiddappa H D and Khezrianjoo S (2012), Langmuir-Hinshelwood Kinetic Expression for the Photocatalytic Degradation of Metanil Yellow Aqueous Solutions by Zno Catalyst, *Chemical Sciences Journal, vol. 2012: CSJ-85*

Roohani N, Hurrell R, Kelishadi R and Schulin R (2013), Zinc and its importance for human health: an integrative review, *Journal of Research in Medical Sciences 18(2):144-157*

Shao R, Sun L,Tang L and Chen Z (2013), Preparation and characterization of magnetic core-shell $ZnFe_2O_4$/ZnO nanoparticles and their application for the photodegradation of methylene blue, *Chemical Engineering Journal 217 185-191*

Srinivasan S.S., Wade J, and Stefanakos E. K. (2006), Synthesis and Characterization of Photocatalytic TiO2- $ZnFe_2O_4$ Nanoparticles, Hindawi Publishing Corporation, *Journal of Nanomaterials, Article ID 45712, Pages 1–4*

Sun L, Shao R, Tang L and Chen Z (2013), Synthesis of $ZnFe_2O_4$/ZnO nanocomposites immobilized on graphene with enhanced photocatalytic activity under solar light irradiation, *Journal of Alloys and Compounds 564 55–62*

Sun S, Yang X, Zhang Y, Zhang Y, Ding J, Bao J And Gao C (2012), Enhanced Photocatalytic activity of sponge-Like $ZnFe_2O_4$ Synthesized by solution combustion method, *Materials International 22(6):639–643*

Sutka A, Parna R, Kleperis J, Kaambre T, Pavlovska I, Korsaks V, Ladole C.A (2012),Preparation and Characterization of Spinel Zinc Ferrite $ZnFe_2O_4$, *International Journal Chemistry Science: 10(3), 1230-1234*

www.americanelements.com accessed 8/4/2015

www.cenbank.org/rates/ExchRateByCurrency.asp, accessed 03/12/2014

www.intechopen.com accessed 6/7/2016

www.oilsplat.wordpress.com accessed 13/04/2015

www.researchgate.net accessed 6/7/2016

www.us-nano.com/inc/sdetail/370 accessed 14/04/2015.

Zhou, A., Peng, J., Chen, Z.,Guo, Z., Ren,N., and Wang,A (2012). Statistical Optimization of Operating Parameters for Enhanced Naphthalene Degradation by Photocatalyst. *International Journal of Photoenergy.*